metals

MDPI

Review

Graphene Family Nanomaterial Reinforced Magnesium-Based Matrix Composites for Biomedical Application: A Comprehensive Review

Somayeh Abazari [1], Ali Shamsipur [1], Hamid Reza Bakhsheshi-Rad [2,*], Seeram Ramakrishna [3] and Filippo Berto [4,*]

1 Department of Materials and Metallurgical Engineering, Amirkabir University of Technology, Tehran, Iran; Somayeh.abazari@gmail.com (S.A.); shamsipur@aut.ac.ir (A.S.)
2 Advanced Materials Research Center, Department of Materials Engineering, Najafabad Branch, Islamic Azad University, Najafabad, Iran
3 Nanoscience and Nanotechnology Initiative, National University of Singapore, 9 Engineering Drive 1, Singapore 1157, Singapore; seeram.rk@gmail.com
4 Department of Mechanical and Industrial Engineering, Norwegian University of Science and Technology, 7491 Trondheim, Norway
* Correspondence: rezabakhsheshi@gmail.com or rezabakhsheshi@pmt.iaun.ac.ir (H.R.B.-R.); filippo.berto@ntnu.no (F.B.); Tel.: +989131704668 (H.R.B.-R.); +4748500574 (F.B.)

Received: 17 June 2020; Accepted: 20 July 2020; Published: 25 July 2020

Abstract: Together with the enhancement of the load-bearing implant process for bone substitution and reproduction, an increasing requirement was observed concerning biodegradable magnesium and its alloys with lighter density and outstanding characteristics. Regardless of the current great potential of Mg utilization currently, the broader use of Mg alloys continues to be constrained by several natural causes, such as low resistance of corrosion, inadequate mechanical integrity during the healing process, and poor antibacterial performance. In this perspective, Mg-based composite encapsulated within graphene family nanomaterials (GFNs) such as graphene (Gr), graphene oxide (GO), graphene nanoplatelets (GNPs), and reduced graphene oxide (rGO) as reinforcement agents present great antibacterial activity, as well as cellular response and depicted numerous benefits for biomedical use. Magnesium matrix nanocomposites reinforced with GFNs possess enhanced mechanical properties and high corrosion resistance (low concentration graphene). It is worth noting that numerous elements including the production technique of the Mg-based composite containing GFNs and the size, distribution, and amounts of GFNs in the Mg-based matrix have a crucial role in their properties and applications. Then, the antibacterial mechanisms of GFN-based composite are briefly described. Subsequently, the antibacterial and strengthening mechanisms of GFN-embedded Mg-based composites are briefly described. This review article is designed to wrap up and explore the most pertinent research performed in the direction of Mg-based composites encapsulated within GFNs. Feasible upcoming investigation directions in the field of GFN-embedded Mg-based composites are discussed in detail.

Keywords: magnesium; graphene; composite; fabrication process; biological characteristics; mechanical properties; corrosion behavior

1. Introduction

The requirement for impressive metallic biomaterials for synthetic implants is mounting continuously and is anticipated to increase to meet the requirements of consumers with bone injuries and deterioration resulting from accidents, sports-related accidental injuries, or the typical course of

aging, which generally require biomaterial implants to recover functionality [1]. Numerous studies were carried out on biodegradable implants, referred to as "smart" implants, in recent years. The primary benefit of biodegradable implants is their degradation characteristic in the simulated body fluid (SBF) solution [2]. The most effective choice provided by this kind of material is that non-degradable implants might be employed in one clinical procedure, and when the devices turn out to be ineffective, they could possibly totally disappear [3,4]. One of the drawbacks of this kind of a treatment is that as soon as the tissue is sufficiently treated, an additional operative treatment pertaining to eliminating the implant ought to be carried out; however, biodegradable implants tend not to need this operation [3,5]. Consequently, issues (such as permanent endothelial dysfunction, long-term physical discomfort, and persistent inflammatory local responses) resulting from non-degradable implants tend to be diminished or vanish [2,6]. Biodegradable implants possess the capability to offer short-term support throughout the healing process to totally substitute a diseased structure of the entire body [7–10]. Recently, attention toward establishing temporary support implants including cardiovascular stents and orthopedic products has increased dramatically [9,11]. In this connection, polymers are exceptional in the current medical industry, and Mg-based, Fe-based, and Zn-based alloys possess greater capability as biodegradable materials pertaining to load-bearing purposes due to the fact that they concurrently possess strength and ductility in comparison with polymers [12,13]. Biodegradable polymers including poly-glycolic acid and poly-lactic acid are typically employed as biodegradable implant materials. The weak mechanical strength of these kinds of polymers considerably lessens their load-bearing and tissue-assisting abilities [14,15]. Commonly, degradable biomaterials need to possess adequate strength, a matching degradation rate with tissue healing rate, and great biocompatibility. The elastic modulus of magnesium (41–45 GPa) in contrast to iron (211.4 GPa) or zinc (90 GPa) is more comparable to natural bone (3–20 GPa) [16]. When the elastic moduli are mismatched, the implant bears a considerably greater part of the load, which results in stress shielding of the bone [3,16]. Furthermore, Mg engages effectively in the bone mineral surface response, which leads to bone proliferation and reconstruction [4,17]. Furthermore, Mg exhibits great biocompatibility along with biodegradability for implant purposes, which causes the elimination of an additional operation to remove the implant [18]. Nevertheless, Mg-based alloys are generally not extensively employed due to their inferior corrosion resistance as a result of their high reactivity. Hence, considerably more consideration ought to be paid to the corrosion resistance of magnesium, which is a crucial concern [3,13]. The need pertaining to lightweight and high-strength materials has resulted in the establishment of metal matrix composites (MMCs) [9,19].

The size of reinforcing agents seems to have a significant influence on the mechanical characteristics of fabricated composites. Regarding the composites incorporated with ceramic reinforcing agents, both the tensile strength and ductility reduce with the increasing particle size of reinforcing agents [20]. The mechanical properties of MMCs might be furthermore amplified by lessening the size of reinforcing agents from the micro- to nano-meter scale, creating the "nanocomposite" specimens [21–26]. With the introduction and rapid growth of nanotechnology, numerous kinds of nanocrystalline materials have already been created [27]. The implementation of nanotechnology in materials science and engineering creates new possibilities and study paths pertaining to the production of new metal matrix nanocomposites (MMNCs) [28]. Nanomaterials with distinctive properties present excellent prospects for use as the reinforcing materials of metals [27].

Nano-sized reinforcement agents present great possibilities to improve the mechanical characteristics of metal matrices according to the Orowan equation and load-transfer strengthening mechanisms [29,30]. Currently, carbonaceous nanomaterials such as graphene and carbon nanotubes (CNTs) appear as essential types of novel materials for structural engineering and practical product applications as a result of their remarkable mechanical characteristics along with outstanding electrical and thermal properties. Associated with numerous nano-additive phases (reinforcements), graphene, an innovative two-dimensional (2D) material, has captured the consideration of researchers because it is characterized as a single atomic layer of sp^2 bonded carbon atoms [12]. Single layer or few layer GNPs

elevate the ductility of metal matrices as they demonstrate outstanding mechanical characteristics and have a lower inclination to agglomerate in comparison with other carbon nanomaterials including CNTs and ball-shaped fullerenes [22,23]. Graphene has distinctive characteristics that allow it to be more useful. First of all, it has substantial stability in chemical and thermal circumstances [31]. Subsequently, an intuitive penetration barrier among the protected metal and reactants might be created through the surfaces of the sp^2 carbon allotropes [32,33]. It was likewise revealed [34] that the bacterial cytotoxicity of GFNs could be assigned to both membrane and oxidative stress. The GFNs are inclined to trigger cellular deposition, since it is more probable to interact with bacterial cells as a result of its greater density of functional groups (FGs) and small size [35]. The GFN nanosheets may destroy the cell caused by stress induction of its membrane layer, which results in interrupting and destroying the cell walls [34]. Consequently, it is crucial to evaluate the latest studies in these fields and sum up their results. Figure 1 [31] depicts a schematic regarding some applications of GFNs including biosensors, phototherapy, tissue engineering (TE), gene and drug delivery, and the formation of coating layers on metallic implants. In this review article, we summarize the mechanical, corrosion, and biological characteristics of recent studies regarding Mg-based matrix composites containing GNPs. We additionally offer our points of views on the forthcoming fabrication methods and development of Mg-based matrix composites containing GFNs pertaining to biodegradable implant purposes.

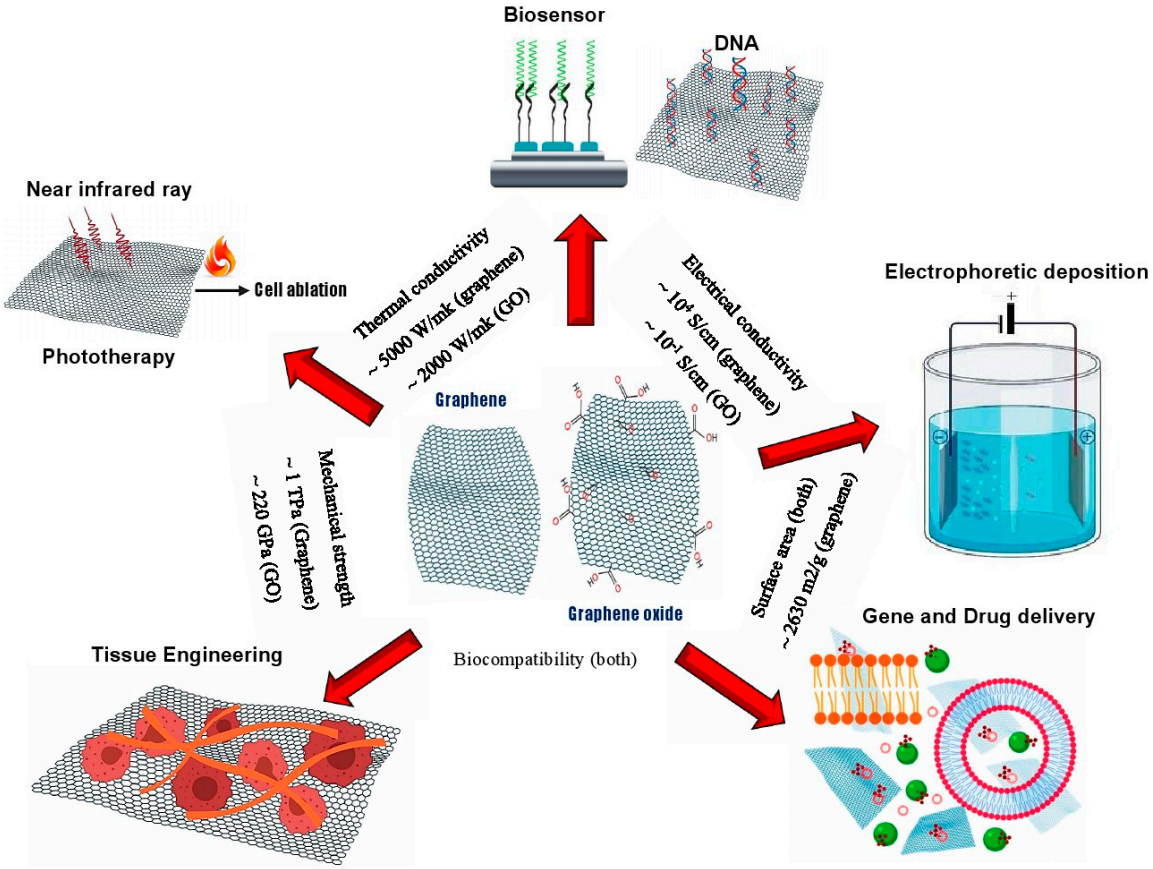

Figure 1. Schematic representation of some of the application of graphene family nanomaterials (GFNs) reproduced from [31], with permission Elsevier, 2019.

2. Development of Mg-Based Biodegradable Metals

Magnesium and its alloys tend to be extremely lightweight metals with density varying from 1.74 to 2.0 g/cm^3, which is certainly lower in comparison with the non-degradable Ti alloy (4.4–4.5 g/cm^3) and almost similar to bone (1.8–2.1 g/cm^3) [14]. The fracture toughness of magnesium is more significant in comparison with ceramic-based components, although the elastic modulus (41–45 GPa) is similar

to bone, a fact that reduces the risk for stress shielding occurrence. Mg is fundamental to human metabolism and is a plentiful cation in the body system, with approximately 25 g Mg saved in the body system and roughly a part of the total content saved in bone tissue. Mg is likewise a cofactor for numerous enzymes and stabilizes the structures of DNA and RNA [14,36]. Magnesium is a kind of active metal with high corrosion potential (−2.37 V), and pristine magnesium metal reveals actually a lower anticorrosion property in the SBF solution with Cl^- [37]. To address this issue and extended the applications of Mg-based alloys, several approaches have been considered including alloying, heat treatment and cold/hot working, powder metallurgy (PM), and surface treatment. Among these, Mg-based composites fabricated with the PM method present versatile mechanical and anticorrosion characteristics attained via the choice of the range of the reinforcement phase.

In this context, Mg and its alloys have been examined as implant materials for several human trials since 1878, which continue to be reviewed by Witte [38] in terms of their historical background. Nevertheless, industrial implant products are not really accessible on the medical market. The historical background concerning clinical examination of Mg-based orthopedic devices since 1900 is shown in Figure 2 [39]. Up to 1980, Mg-based materials were typically priced too high to manufacture; a feasible fabrication process and the resulting mechanical characteristics were restricted; and numerous unsettled issues in connection with the high corrosion rate remain. It is shocking that in the previous decades, no clinical trial report was found regarding Mg pertaining to implant applications [30,39]. Currently, there is a new anticipation pertaining to a wide range of novel technologies regarding Mg alloys' utilization in mass production. There is certainly a demand for a novel class of biomaterials for revolutionary implants and tissue scaffolds that should be in a position to promote the healing rate of damaged tissues at the molecular level [40–44]. In numerous situations, the body requires an implant merely for short-term applications, wherein materials presenting a biodegradable behavior are considered a better strategy compared to stable and inert ones. The perfect biodegradable material, for instance in bone reproduction methods (polymer, ceramic, metal, or composite), has to offer sufficient mechanical fixation, full degradation at the time when it is no longer required, and total substitution by fresh bone tissue [44].

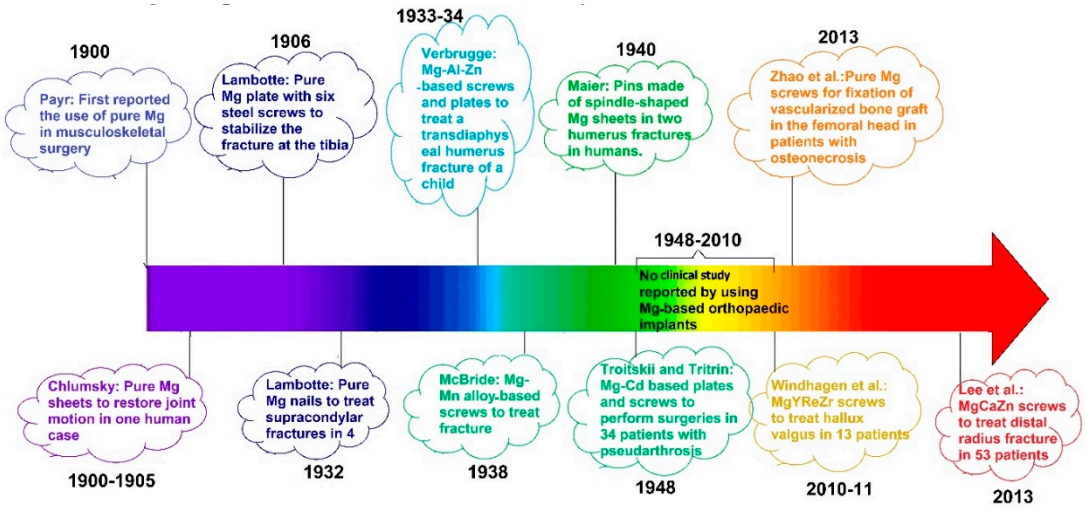

Figure 2. Historical background concerning clinical examination of Mg-based orthopedic devices reproduced from [39], with permission from Elsevier, 2017.

3. Mg-Based Biocomposites and Bio-Alloys

Mg-based bio-alloys are considered to degrade throughout the body system at a suitable degradation rate; however, they likewise possess the issue of a rapid degradation rate throughout tissue regeneration, which restricts their use for clinical purposes [45]. Mg-based alloys likewise are considered as a great option in the areas of tissue engineering, orthopedics, and cardiovascular stents

as a result of their appropriate mechanical characteristic, cytocompatibility, and suitable corrosion rate [46]. The biocompatibility of a metallic biomaterial is its capability to function with an appropriate host reaction throughout its designed clinical utilization in a body system. The interaction between host tissue, the performance of the metallic implant, and its material characteristics regulate the biocompatibility of an implant, as demonstrated in Figure 3 [47]. The biological reaction of this kind of implant might alter with any specific post-implantation modifications in the host tissue. These biological reactions rely on the chemical and physical characteristics of an implant, the kinds and regions of host tissues that are subjected to an implant, the length of the exposure, the implant's surface characteristics, structure, and forces employed on synthetic implant, and the physical performance for which the particular metallic implants was initially chosen [47].

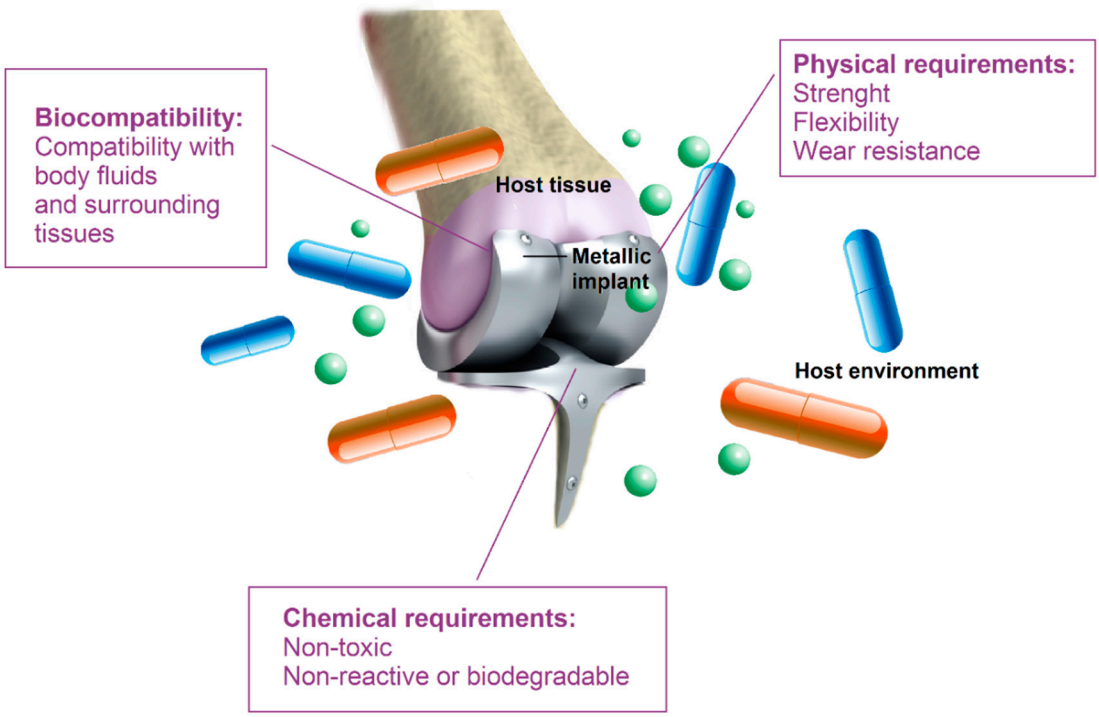

Figure 3. Characteristics of metallic materials regulating the cellular response of an artificial implant reproduced from [47], with permission from Wiley, 2019.

Despite the fact that Mg-based bioalloys have considerable properties, it is still required to enhance the mechanical characteristics to maintain their strength throughout the incubation period. Magnesium possesses a hexagonal close packed (HCP) structure, which has a restricted number of slip systems and, for that reason, presents a brittle behavior. This is essential to increasing the ductility of Mg materials with little or no effect on strength. Therefore, nanocomposites may boost the strength and ductility at the same time [45]. The appropriate option for reinforcements, their grain size, and their natural biocompatible characteristics can achieve the greatest degree of mechanical and anticorrosion properties and a great cell response. The composite materials consist of a minimum of two materials, which are known as the matrix and reinforcement. All the materials of the composite ought to be cytocompatible and not induce toxicity in any SBF solution. The composite material permits the mixture of the matrix and reinforcement properties including great mechanical characteristics (compressive strength (CS) and tensile strength (TS)), high anticorrosion performance, and biocompatibility. The choice of matrix component and reinforcement component is extremely vital to attain the desirable characteristics [45].

Experts have employed new ideas to enhance the mechanical properties, corrosion performance, and biocompatibility of these materials, which are extensively reviewed due to the stability of Mg-based materials in the biomedical area. Carbon-based materials display a broad variety of

distinctive characteristics, such as a great aspect ratio, an outstanding high Young's modulus and strength, as well as remarkable electrical and thermal characteristics. These outstanding properties have resulted in the employment of carbonaceous nanomaterials as the reinforcements for polymers, ceramics, and MMC for their distinctive characteristics [27]. The characteristics of GFN-associated components and their capabilities to be functionalized and coupled with biomolecules and materials provide numerous possibilities to offer biocomposites with tailored characteristics, as presented in Figure 4.

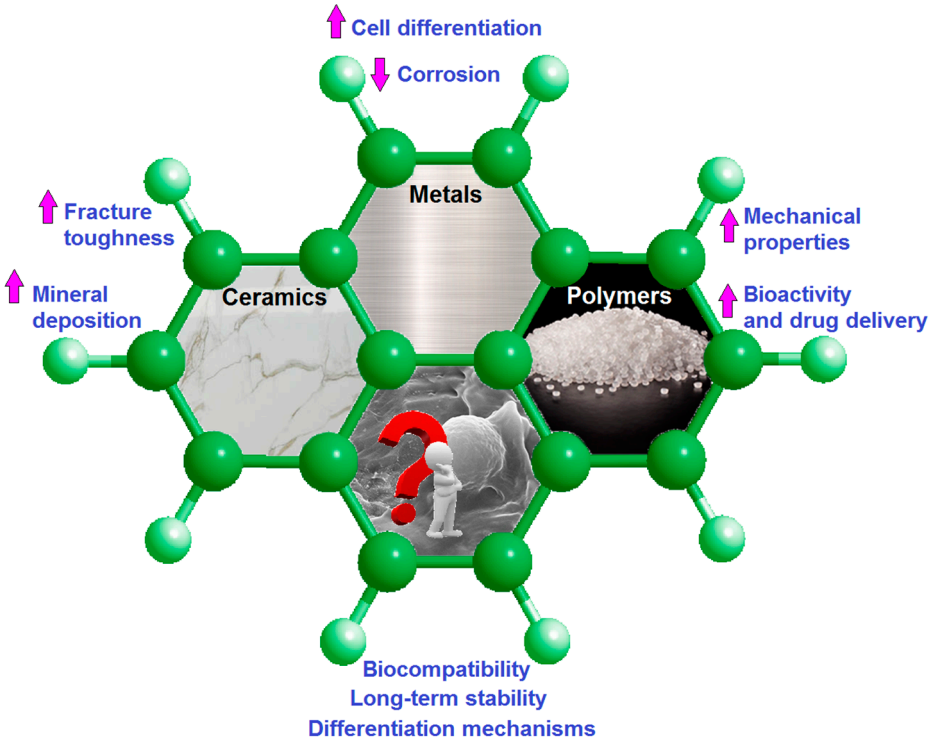

Figure 4. Potential enhancements offered by GFNs in biomaterials and essential aspects to be designed to translate the biocomposites to clinical examination.

4. Graphene Family Nanomaterials

Despite the fact that composite materials can offer a number of positive aspects that single-component materials cannot, they could possibly likewise offer features that need more enhancements. As an illustration, ceramic-polymeric composites might be bioactive, whereas they could result in sensitive responses and offer minimal mechanical characteristics [48]. Even with the latest developments, the progress of novel materials and approaches to produce the new class of biocomposites with enhanced features is being given great attention [49]. Metals are employed for a number of biomedical purposes in neat form or as alloys because of their great toughness and stiffness. The Gr-family components might enhance the characteristics of metals even more and present a bioactive character to the metal-based composites.

As a new nanomaterial family, GFNs demonstrate outstanding capabilities against a wide range of bacteria including Gram-positive and -negative bacteria [31]. Single-GFN and GFN-based composites exhibit obvious antibacterial functionality. Furthermore, the reasonable design of GFN-based composites might improve this particular potential. A comprehensive overview of single-GFNs' antibacterial functionality is presented in Table 1. The antibacterial activity of Gr was first documented in 2010 [50,51], where graphene was observed to significantly destroy and cause the dysfunction of the bacteria attaching to it [51]. This antibacterial approach was effective and fast for *Escherichia coli* (*E. coli*) and *Staphylococcus aureus* (*S. aureus)*, and destruction was observed to primarily take place in

the cell membrane. A test disclosed that graphene nanosheets actually possessed a greater antibacterial activity in comparison with conventional antibiotics, including kanamycin [52]. Similar to Gr, GO also exhibits an outstanding bactericidal capability for a wide range of bacteria [51]. Gr is a plane of carbon atoms, and GO is an oxidized Gr sheet with numerous oxygen-containing FGs [53]. Right after reducing the functional oxygen-containing groups, GO will certainly turn out to be rGO. Commonly, rGO nanosheets tend to be reduced through hydrazine [51] and dithiothreitol [54]. Bacteria were suggested to reduce GO by means of the metabolism of glycolysis in a self-limiting fashion [55]. Neat Gr spread out with complications in the solutions (aqueous and organic) as a result of the insufficient hydrophilic groups. On the other side, GO and rGO demonstrate a particular amphiphilicity (lipophilic and certainly hydrophilic) because of the amount of extra FGs [31].

Table 1. The antibacterial effect of the single-graphene family of nanomaterials (GFNs) on bacteria.

Material	Fabrication Method	Bacteria Strains	Killing Rate	Incubation Time (h)	Material Concentration (mg/L)	cfu/mL	Ref.
Gr	Chemical exfoliation	*Escherichia coli* (*E. coli*)	59%	1	-	10^8	[51]
Gr	Chemical exfoliation	*Staphylococcus aureus* (*S. aureus*)	74%	1	-	10^8	[51]
rGO	Hummers and Offeman	*E. coli*	88%	4	100	10^6	[51]
rGO	Hummers and Offeman	*E. coli*	81%	2	150	10^6–10^7	[51]
GO	Chemical exfoliation	*E. coli*	84%	1	-	10^8	[54]
GO	Chemical exfoliation	*S. aureus*	95%	1	-	10^8	[54]
GO	Modified Hummers	*Fusarium graminearum* (*F. graminearum*)	90%	7	500	3×10^7	[56]
GO	Modified Hummers	*Fusarium oxysporum* (*F. oxysporum*)	80%	7	500	3×10^7	[56]
GO	Modified Hummers	*E. coli*	69%	2	80	10^6–10^7	[57]
GO	Hummers and Offeman	*Xanthomonas oryzae pv. oryzae* (*X. o. pv. oryzae*)	100%	4	250	10^7–10^8	[58]
GO	Modified Hummers	*Activated sludge*	35%	5	100	5×10^5	[59]
GO	Hummers and Offeman	*Pseudomonas aeruginosa* (*P. aeruginosa*)	100%	2	175	10^6	[60]

Gr is another appealing and distinctive crystalline allotrope of carbon that demonstrates 2D properties. It is regarded as the initial 2D material [61,62]. In this regard, Figure 5 exhibits the historical background and development stages of Gr formation [49]. Gr was identified in 2004 by Geim and Novoselov [62]. They effectively separated graphene through mechanical exfoliation of graphite crystals employing the cohesive tape approach. Their breakthrough was recently privileged with the 2010 Nobel Prize in Physics. Nevertheless, the low efficiency of this particular approach causes it to be inappropriate for large-scale manufacturing purposes. The essential advancements in relation to GFNs, in particular Gr, are described pictorially in Figure 5. Gr might be generated by four approaches: (1) CVD [63]; this research that commenced in the 1970s was accompanied by a considerable amount of studies conducted by surface researchers on monolayer graphite [64]; (2) epitaxial growth of the Gr layer by electrically insulating substrates [65]; (3) mechanical exfoliation of Gr from bulk graphite (e.g., using Scotch tape); and (4) reduction of graphene derivatives including GO [66,67]. The latter approach exhibits possibilities pertaining to the manufacturing of graphene sheets in the mass amounts that are

required for applying it to composites. GO sheets might be taken out of "graphite oxide (GRO)", which is commonly prepared through the oxidation of graphite [68,69]. GRO could be entirely exfoliated to create an aqueous solution of GO sheets by sonication [61]. Extensive investigation [70] on these kinds of aqueous solutions was performed in the 1950s and the 1960s. Chemical reduction of GO in colloidal suspensions might be conducted to fabricate massive volumes of chemically modified graphene (CMG) sheets [61,71], which are appropriate for compositing purposes. Thermal reduction of GRO is a different method that is usually employed to attain massive volumes of Gr platelets. Fast heating (> 2000 °C/min) up to 1050 °C exfoliates, as well as reduces GRO [61,72,73]. However, GO and rGO are usually manufactured through relatively inexpensive chemical approaches employing graphite as the basis material [74–77]. They are usually distributed evenly in stable aqueous solutions to construct macroscopic structures at commercial-scale [76,78].

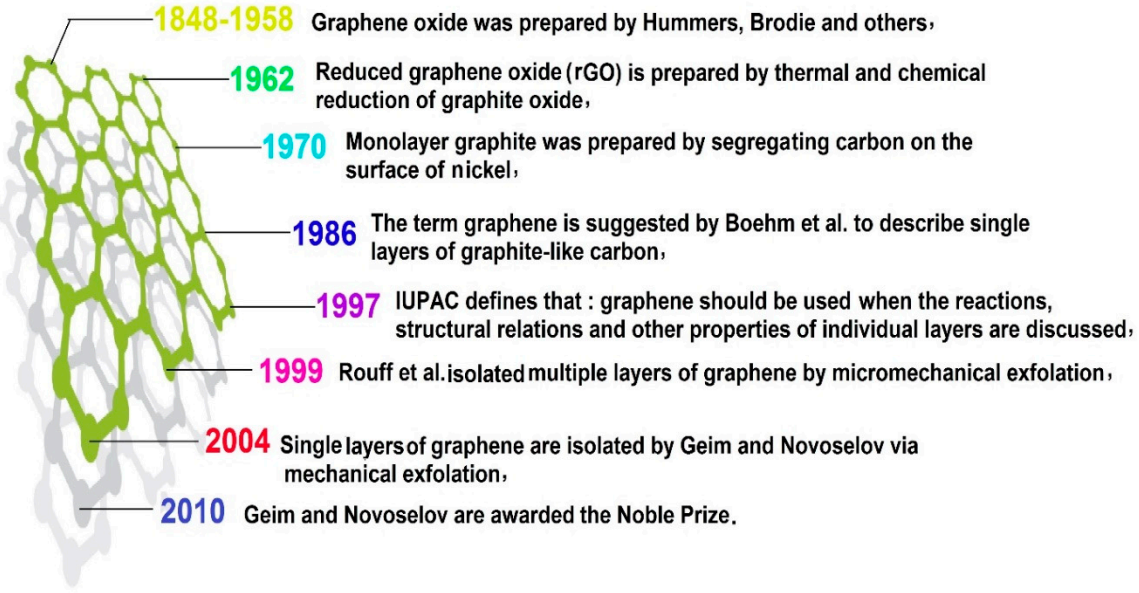

Figure 5. Historical background and development stages of GFNs' formation reproduced from [49], with permission from Elsevier, 2017.

Gr also offers a fracture strength of 130 GPa, a Young's modulus of 1 TPa, a low density of 1 g/cm^3, and a great specific surface area that might enable it to be a remarkable reinforcement intended for MMC [79,80]. The reason behind the great stiffness and elastic strength is the Sp^2 hybridized and covalently bonded C-atoms in a hexagonal network. Furthermore, graphene might experience substantial elastic strains up to 15% [81]. The issues including insufficient bonding at the Gr/metal interface lead to the poor interface adhesion and decrease the mechanical characteristic of the metal matrix resulting from the elastic incompatibility [82,83]. Moreover, Gr has more difficulty in spreading out in comparison with other reinforcements, as a result of its interfacial contact region [83]. The maintenance of the integrated structure of GNPs is the essential matter due to the fact the more complete the structure of the GNPs is, the greater and considerably more productive the bearing potential of GNPs might be in the matrix throughout a loading procedure. Thus, composites might attain greater strength and modulus and considerably more issues in elastic deformation [84].

5. Fabrication of Graphene-Mg MMNCs

Magnesium MMCs present versatile mechanical and anticorrosion characteristics as obtained via the choice of the range of the reinforcement phase. The amount, dispersion, and size of the reinforcements are key elements regarding the mechanical performance and degradation rate of Mg MMCs. Numerous reinforcements were used to fabricate Mg MMCs, including Ca-P- and bioglass (BG)-based ceramic [85–88], ZnO [25], and Ca particles [89], by means of powder metallurgy (PM) and

stir casting (SC) methods. In this context, it was suggested that the uniform distribution of GNPs in the metal matrix is a crucial issue throughout the fabrication of composites. The thickness of GNPs with joint stacked sheets is hence considerably greater in comparison with an individual graphene sheet. GNPs are usually effortlessly dispersed in any kind of solvent and matrix. The Mg-GFs nanocomposite is usually manufactured through employing various manufacturing approaches including disintegrated melt deposition (DMD), stir casting, liquid infiltration, gravity casting, melting, PM, and semi-powder metallurgy (SPM). Nevertheless, current research reveals that PM coupled with the hot extrusion (HTE) procedure and SPM is one of the successful approaches to achieve the appropriate mechanical characteristics. Traditional manufacturing approaches, for example stir casting, are not able to address this issue [83].

5.1. Powder Metallurgy

The PM approach is an adaptable method for fabrication of Mg-based composites with GFN nanofillers because of its ease of use, overall flexibility, and close proximity to net-shaped functionality, as shown in Figure 6. The procedure consists of mechanical mixing of nanofillers with metal/alloy powders in a rotary mill, accompanied by sintering and various types of densification approaches including cold isostatic pressing (CIP), hot pressing/hot isostatic pressing (HP/HIP), or spark plasma sintering (SPS). In particular circumstances, extra mechanical deformation modifications including HTE, HF (hot forging), hot rolling (HR), friction stir processing (FSP), and equal channel angular processing (ECA) approaches are employed to additionally compact them into full-compact nanocomposite specimens. With the PM approach, which consists of three fundamental stages (blending, densification, and sintering), a homogeneous and even distribution of reinforcing agents within the matrix alloy has been accomplished [90,91]. The HTE procedure is applied to enhance the densification of composites due to the fact that it is complicated to avoid the creation of micropores in the composite following sintering [92,93]. This review article describes the current trends in processing and the mechanical and anticorrosion characteristics of Mg-based alloys incorporated with Gr-family nanomaterials.

The accomplishment of a uniform additive phase via simply blending metal powders with carbon-based components is fairly inadequate, as anticipated. By utilizing a ball mill or mechanical alloying (MA) approaches, a greater distribution of additive agents is usually obtained. Nevertheless, the handling methods must be done with care in order to maintain the structural integrity of carbon-based components. This is due to the fact that the long-term ball milling procedure might damage the crystallinity of carbon-based components [27]. A number of authors used a traditional mixed press-sinter method to fabricate the MMCs. Incorporation of Gr-family nanomaterials into Mg matrix improves the thermal conductivity, and GNPs are likewise great additive agents for strengthening the mechanical performance of the Mg composite. Furthermore, Mg is generally defined as a light metal; it is typical used in the vehicle and aviation industrial sectors to be able to lessen fuel usage. Thus, the manufacturing and advancement of Mg-GNP composites are extremely crucial. Shahin et al. [94] employed MA methods to spread out 0.5 wt.% and 0.1 wt.% Zr and GNPs, respectively, in the Mg matrix. The blend's powder was subsequently cold pressed and sintered at 760 MPa and 610 °C respectively to obtain the nanocomposite. Their outcome revealed that the Mg and Zr powders showed an irregular flake-like shape, even though Gr powders presented a flake-like shape along with wrinkled edges and a particle size of 15 μm.

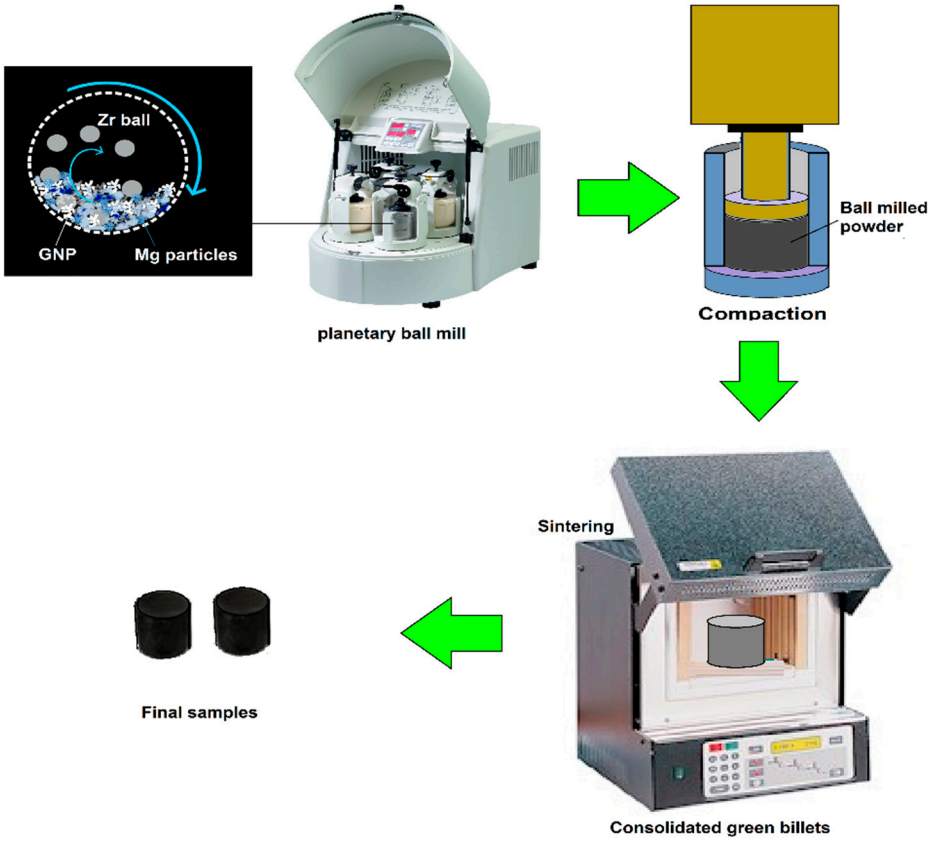

Figure 6. Illustration of the powder metallurgy method for manufacturing Mg-based composites with GFN nanofillers.

5.2. *Stirring Casting*

PM approaches are quite costly and might lead to the destruction of additive phases throughout the ball milling procedure, which will ultimately have an effect on the mechanical characteristics of the produced composites. On the other side, the stir casting approach is desirable because of numerous benefits compared to the PM approach. For instance, the stir casting approach is more affordable, and porosity forms as a result of the solidification shrinkage, while hydrogen generation is extremely low. In addition, a broad range of patterns and sizes (of matrix and additive phases) can certainly be employed. The additive phases do not cause any damage, and virtually any type of matrix/reinforcement is usually applied regardless of the melting points [95]. An additional method for MMCs' advancement is to embed the additive phases into the melt accompanied by the stirring casting approach. Typically, bioceramic or BG is chosen to be the additive phases; however, the weak wettability of the bioceramic restricts the content of additive phases, besides the distribution of the additive phases. A number of approaches has already been performed to overcome this restriction of the SC approach. Du et al. [92] evaluated the strengthening mechanism of Mg (ZK60)-GNP composites fabricated via melting stirring accompanied by the HTE procedure. Homogeneous dispersion of GNPs in the ZK60 matrix was obtained via a melting mixture approach. Moreover, GNP embedding in ZK60 matrix led to increasing both the tensile and compressive strength. Overall, the PM method following the HTE procedure leads to enhancement of the mechanical characteristics of MMCs. In contrast to PM MMCs, which possess a lower than 0.5% porosity because of the HTE procedure, the semi-solid cast composite was observed to be microporous, hence suggesting a higher degradation rate in comparison with the PM coupled with HTE procedure [96]. In this context, Ramezanzade et al. [96] prepared Mg-based composites by embedding various contents of GNPs (0.1, 0.2, and 0.4 wt.%) as additive agents via an SC method accompanied by homogenization and extrusion in an effort to strengthen the mechanical characteristics of the Mg-based alloy. Their outcome showed that embedding 0.2 wt.%

GNPs into the Mg-based alloy resulted in grain refinement (36%) and the lessening of anisotropy (14%), as well as a reduction of twin formation. The homogeneous distribution of GNPs accompanied by enhanced non-basal slip and grain refinement enhanced the tensile fracture strain.

5.3. Disintegrated Melt Deposition

Materials researchers have invested substantial effort by presenting enhanced melt procedures to be able to accomplish a greater distribution of GNPs in the metal matrix. Wang et al. [97–99] and Rashad et al. [95,100] systematically examined the manufacturing process and mechanical performance of Mg-based composites incorporated with Gr. The DMD approach was implemented to distribute nano-additives in molten Mg alloys [27], as shown in Figure 7. This approach consists of mechanical stirring Mg chips and the nano-additive under a neutral gas (e.g., argon) to cast ingots with the subsequent HTE procedure. Microstructural assessment showed that the extruded composite specimens presented a relatively even dispersion of Gr-family nanomaterials [27].

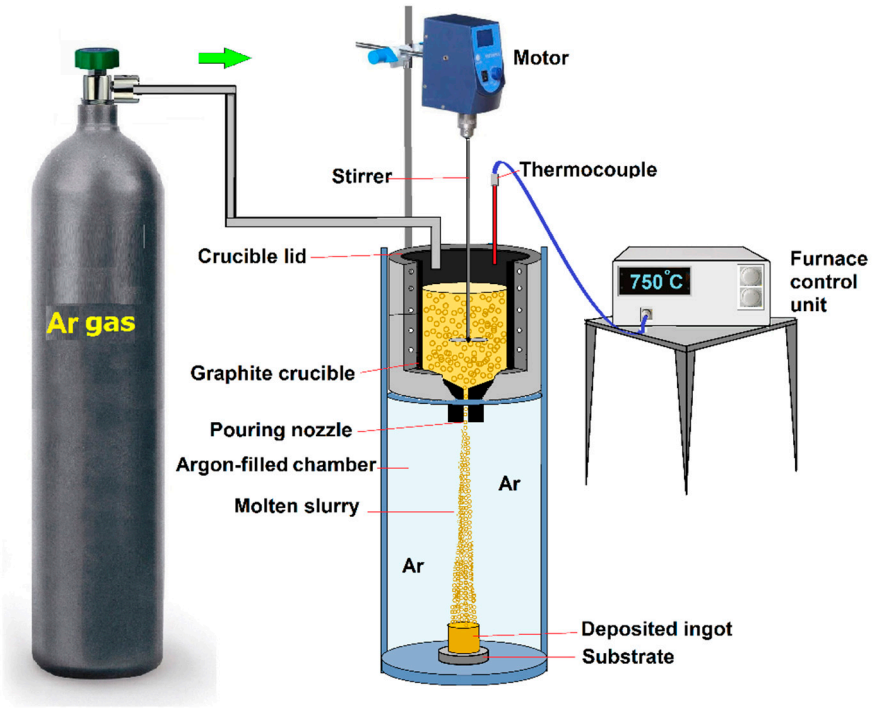

Figure 7. Schematic representation of the disintegrated melt deposition (DMD) process reproduced from [27], with permission from Elsevier, 2013.

Rashad et al. [95] also fabricated Mg alloy-GNP composite via the DMD approach accompanied by homogenization treatment and the subsequent HTE procedure, and their outcomes showed that GNP incorporation had a considerable influence on reducing the grain size and modifying the basal textures because of their homogeneous distribution within the matrix of the Mg-based composite, which led to substantial enhancement of the mechanical properties including the hardness, TS, and CS. Aside from that, the TS of an extruded Mg alloy-GNP composite was also evaluated at higher temperatures, and their result showed that fracture strain increased and TS diminished with increasing testing temperature. The increase of fracture strain at elevated temperature was primarily caused by substantial grain refinement and homogeneous nano-additive dispersion. The fracture surface evaluation showed that deformation potentially took place via grain boundary (GB) moving accommodated via penetration transport. Wang et al. [99] also uniformly dispersed GNPs in the matrix of bare Mg in a dynamic solidification approach. In this approach, via the pre-dispersion procedure, incorporated GNPs split up the agglomerate particles of neat GNPs and maintained the GNPs in a repulsive situation.

This type of distribution resulted in further reducing the grain size and more enhancements of the mechanical properties.

5.4. Friction Stir Processing

FSP is established by the alteration of friction stir welding (FSW) to create a composite with a sub-microstructure close to the surface area of metallic materials via dynamic recrystallization, as demonstrated in Figure 8 [90]. In this approach, a spinning device pin is introduced to the substrate in a way that the friction and plastic deformation caused by the device heat and soften the workpiece. The device pin subsequently stimulates the intermixing of the material in a local area [27]. To manufacture GFN-reinforced composites, numerous holes are initially drilled into a metallic plate accompanied by filling up with GFNs and modifying with subsequent FSP (Figure 8). Arab et al. [101] manufactured a nanocomposite that was prepared via embedding GNPs into AZ31 magnesium alloy via FSP. Traditional FSP samples confirmed a 133% increase in strain-to-fracture, even though it was diminished by incorporating GNPs. Nevertheless, the existence of GNPs elevated the YS and UTS to 217 and 278 MPa, respectively. Chen et al. [17] also successfully fabricated Mg-GNP composite via liquid state approaches followed by solid state stirring. Their approach is schematically revealed in Figure 8. In this procedure, GNPs are incorporated into the molten magnesium via a feeding procedure and subsequently distributed into the molten composite via an ultrasonic procedure for a short time. Microstructural evaluation results revealed that GNPs were not evenly distributed within the Mg-based matrix. To obtain an enhanced distribution of GNPs in the composite, FSP was employed on the surface of the cast specimens. In this regard, FSP led to enhancement of the distribution of GNPs in the matrix of the composite.

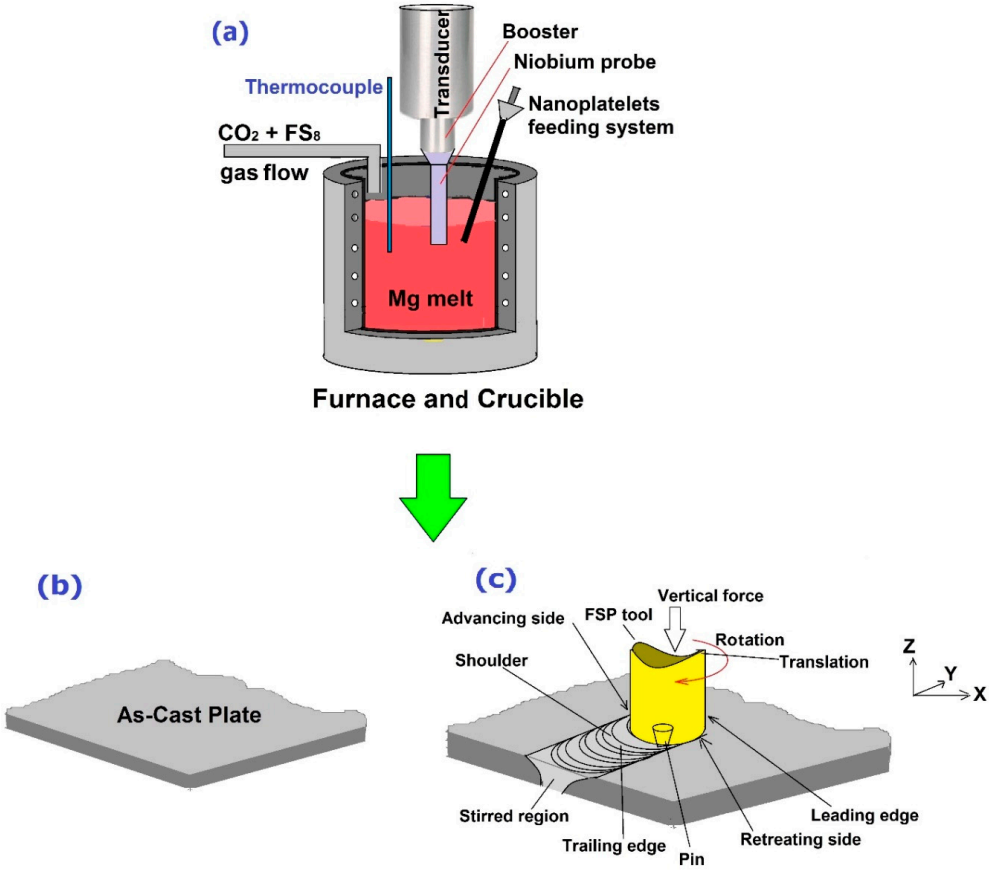

Figure 8. Schematic of the processing procedure for fabricating Mg-graphene composite (**a**) stir casting, (**b**) as plate and (**c**) Friction stir processing (FSP) reproduced from [90], with permission from Elsevier, 2012.

5.5. Selective Laser Melting

The laser deposition approach pertains to utilizing coherent and extreme laser beams for fabricating MMNCs employing metal powders. Laser beams usually have the ability of achieving extremely high-speed rates of surface melting accompanied by solidification at cooling rates of ~107 ks^{-1}. The laser processing approach provides unique benefits regarding creating composites including a short handling period, a reduced amount of distortion of the specimen, and near net shape manufacturing. As shown in Figure 9, SLM was employed by Shuai et al. [102] to also prepare 3D honeycomb nanostructure-embedded Mg alloys, in which the honeycomb nanostructure was reinforced with GO as an additive phase. Results revealed that GO was dispersed within the GBs and progressively wrapped α-Mg grains when the content of GO increased. The close and complete wrapping suggested a beneficial affinity and useful protection of GFNs, for instance GO in Mg-based alloys, against corrosion attack.

Figure 9. Schematic diagram for the preparation of GO reinforced AZ61 magnesium alloy by selective laser melting (SLM) reproduced from [102], with permission from Elsevier, 2019.

5.6. Multi-Step Dispersion Route

Melt stirring is a traditional method for MMC fabrication, while the direct encapsulation of GFNs like Gr (additive phase) into the melt could effortlessly result in carbon float and aggregation because of the layered structure of Gr [100]. To disperse the GNPs effectively into the metals' matrix, the multi-step dispersion route combining different process steps was developed. Xiang et al. [83] encapsulated Mg-based composites with GNPs by employing the multi-step dispersion method comprising pre-dispersion of the additive phase, semi-solid treatment stirring (SSTS), and high energy ultrasonic processing, followed by the HTE procedure, as shown in Figure 10 [83]. Effectively-distributed however non-uniformly dispersed GNPs were attained in the Mg matrix. A perfect distribution of GNPs inside the Mg matrix was because of the existence of carboxyl groups (-COOH) at the edges of GNPs, which were stable in the molten Mg based on the chemical stability of GRO below 1050 °C. Actually, The SSTS inhibited the extreme oxidation of Mg-based chips and the floating of GNPs owing to the lower temperature and the greater viscosity of the semisolid metal in comparison with the liquid state melt. Furthermore, the following processes of SSTS, ultrasonic vibration, and the HTE procedure additionally supported the dispersion of GNPs, as noted in the earlier studies [103,104]. Du et al. [92] synthesized a Mg alloy-GNP composite via melt stirring coupled with the HTE procedure. Prior to melting, GNPs were pre-dispersed inside the Mg matrix under various stirring modes to ensure the suitable distribution GNPs inside the Mg matrix. Their outcome

showed that in contrast to the Mg-based alloy without GNPs, the Mg-based composite containing 0.05 wt.% GNPs had significantly improved mechanical properties.

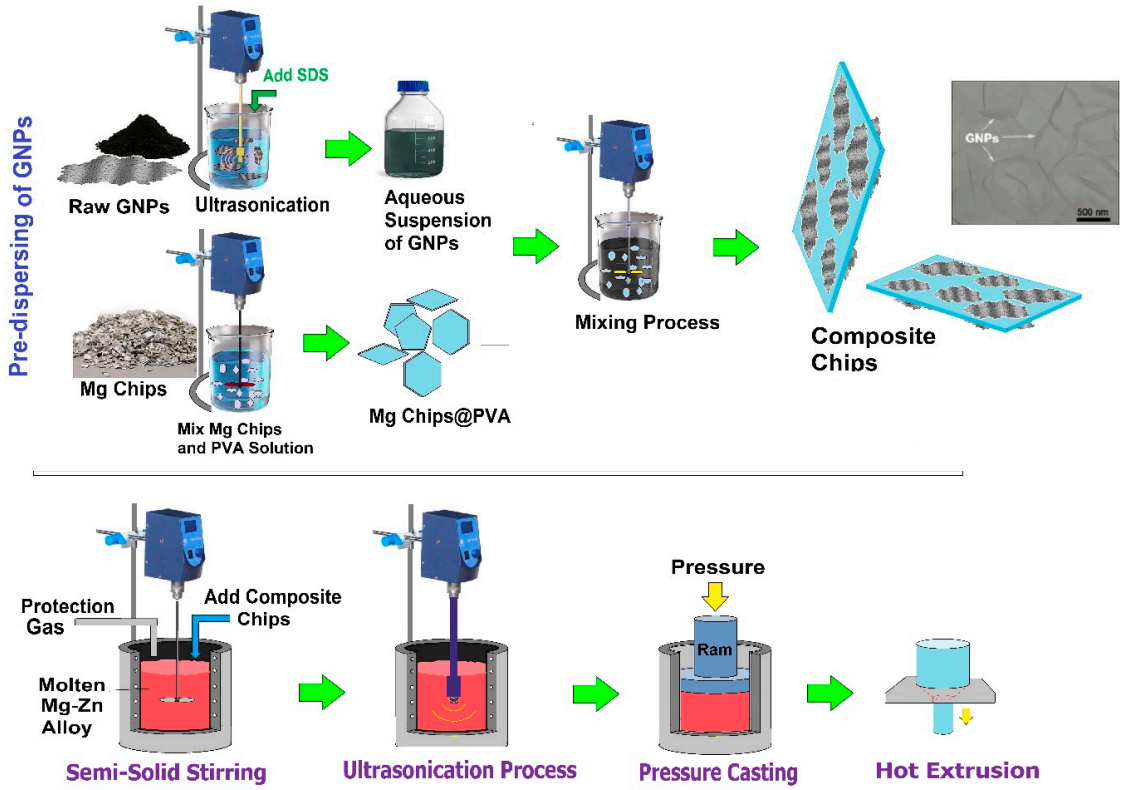

Figure 10. Fabrication route of the Mg-based composite encapsulated within GNPs using the multi-step dispersion route (MSDR) reproduced or adapted from [83], with permission from nature research, 2016.

5.7. Semi-Powder Metallurgy

Rashad et al. [91] performed Mg-GNP composite synthesis by employing the SPM approach. They noticed that the Mg structure was modified because the encapsulation of GNPs had an effect on the mechanical performance of the composite. Turan and coworkers [105–109] likewise investigated the influences of carbon-based additives on the microstructure and properties of Mg-based composites by this approach. The SPM approach provides a homogeneous dispersion of the additive phase in the Mg matrix alloy. This method is free of ball milling since ball milling is regarded as a major issue when employing Mg due to the fact that it generates heat, which might burn the Mg powder readily, as exhibited in Figure 11 [110]. Thus, this approach is used as an alternate choice to ball milling, and it has good possibilities regarding the fabrication of a Mg-based composite, which is regarded as a great candidate for engineering purposes. GNPs are usually distributed in almost all types of solvents and matrices effortlessly in comparison to CNTs. The Mg alloy-GNP composite is manufactured by the semi-powder metallurgy method accompanied by the HTE procedure. Their result exposed the homogeneous distribution of GNPs in the matrix [109]. In this regard, Sabri et al. [110] also synthesized a Mg-based composite by SPM, which was encapsulated within GNPs, and their result revealed that homogeneous and even dispersing of the low amount of GNPs inside the Mg-based matrix led to partial agglomeration of GNPs with better mechanical properties. In the same manner, Rashed et al. [111] utilized a simple approach to enhance the mechanical properties of Mg-GNP composites by intercalating a small amount of MWCNTs among the layers of GNPs. Their outcome demonstrated that that reduction of the grain size did not occur homogeneously within the matrix surface. This could be caused by the weak distribution of 2D GNPs as an additive phase in the matrix. In this view, the microstructure of Mg alloy-CNTs composite shows the presence of micropores on its surface, whereas

Mg alloy/CNTs-GNPs are free of micropores and present great chemical bonding among the additive phase and the matrix. Their outcome likewise confirmed that GNPs as part of GFNs are encapsulated in Mg matrix with outstanding interfacial adhesion without the presence of cracks.

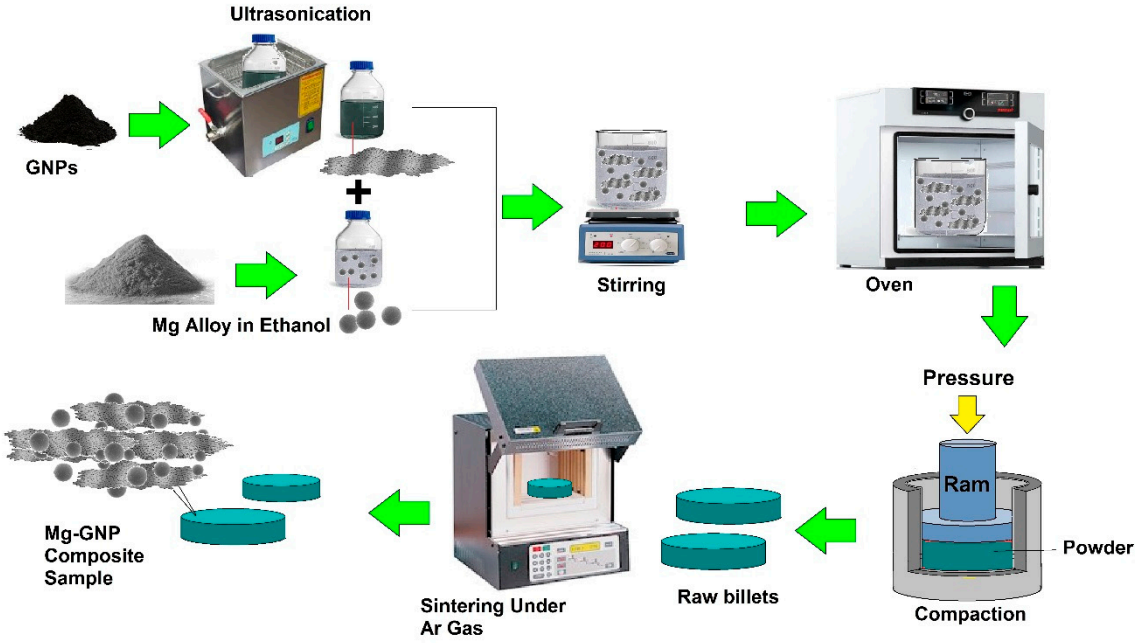

Figure 11. Schematic representation of Semi powder metallurgy (SPM) for synthesis of GNPs reinforced Mg-based composite, reproduced from [110], with permission from Elsevier, 2020.

6. Mechanical Properties of Mg-GNP-Based Composites

The considerable enhancement of the mechanical performance of the Mg-based composite was basically caused by decreasing grain size and close interfacial bonding of GFNs within the matrix. In particular, the wrinkled surface of Gr-family materials like GNPs might result in successful mechanical interlocking with the composite matrix [112]. When a crack grows around the GNPs, the stress in the matrix might be properly shifted to GNPs as a result of the superior elastic modulus of GNPs in comparison with other bioactive ceramics. During this period, GNPs are lengthened and fractured or possibly pulled out through the matrix when going above the greatest interface bonding strength; the mechanisms of pull-out impact, crack bridging, deviation in the path of crack growth, and crack tip blunting via GNPs absorb a great amount of outward energy, although keeping a small amount of energy for additional growth of the crack, as shown in Figure 12. Consequently, the crack grows in a step-like fashion and progressively reduces or possibly ends, in that way enhancing the load-bearing ability of the matrix [32].

There are widely recognized toughening systems for the Mg matrix. These mechanisms are refined grain structure, Orowan looping, solid solution strengthening, precipitation strengthening, stress transfer or load bearing, the coefficient of thermal expansion (CTE), and modulus mismatch toughening [113]. Nevertheless, a uniform dispersion of GNPs within the Mg matrix is not virtually attainable. Moreover, to be able to obtain stress transfer through Mg matrix to GNPs, we require a solid attaching mechanism of graphene to metal [84]. Due to the fact GNPs are a 2D material, the stress transfer toughening system might be among the primary strengthening mechanisms in the Mg matrix strengthened by GNPs [114–120]. The stress that often is employed on the Mg matrix could transfer to the additive phases (GFNs) from the Mg matrix via shear stresses combined with the interface among the Mg matrix and additive phases.

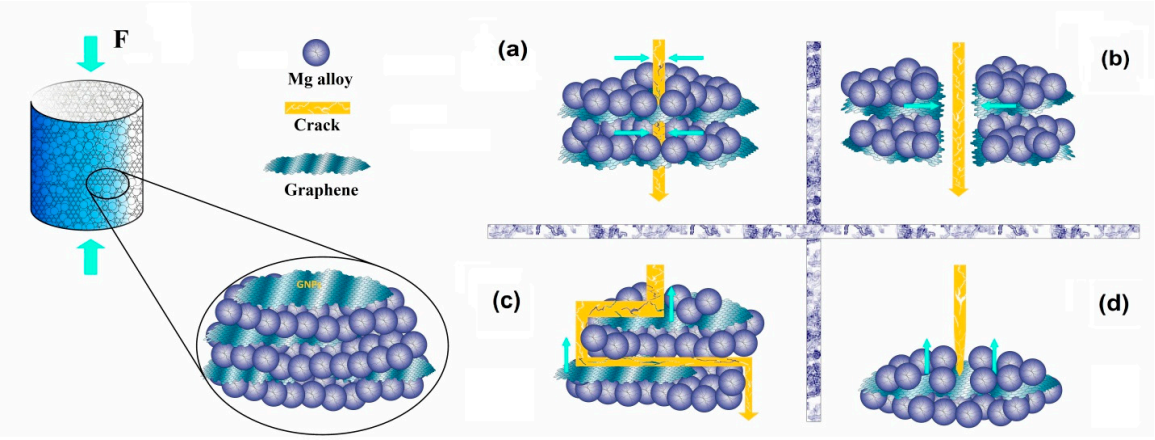

Figure 12. Schematic diagram showing the pull-out (**a**), crack bridging (**b**), crack deflection (**c**), and crack tip (**d**) shielding mechanisms by graphene.

Due to the fabrication technique, the grain size of the Mg matrix reduces. Because of the refined grain structure of the Mg matrix, which leads to enhancement of the strength of the Mg-based composite based on the Hall–Petch formula [92,97,98,113], it is among the primary strengthening systems in the Mg matrix strengthened via GFNs. Aside from that, due to the strain hardening, increasing dislocation amount, and CTE mismatch toughening amplified in the Mg-based composites, this likewise leads to toughening of the Mg matrix strengthened via GNPs [30,90,114,115]. It is worth mentioning that CTE mismatch among the Mg matrix and Gr may result in enhancing the dislocation amounts and increasing the toughness of the Mg-based composites [30,93,116,117]. The CTE mismatch toughening systems in the Mg matrix strengthened by GFNs are determined by the size, morphology, and geometry of the Mg matrix and additive phases. Another toughening system in the Mg matrix strengthened by GNPs is Orowan looping, which was suggested by Rashad et. al. [118,119], where unmodified particles are positioned inside the grains. Hence, the size of grains and additive phases are extremely crucial to obtain the Orowan toughening in the Mg matrix. Residual dislocation loops could be created close to GNPs following a dislocation that bows out and bypasses all of them. Substantial work hardening is usually ordered through these loops [101,120].

Munir et al. [30] examined a Mg-based matrix strengthened with GNPs that were prepared via PM for biomedical purposes. GNPs (5–9 nm layer thicknesses) with various amounts (0.1–0.3 wt.%) were distributed within the Mg-based matrix via the ball milling method. The outcomes revealed that GNPs' incorporation enhanced the mechanical characteristics of Mg through thermal mismatch and reducing the grain size. Furthermore, maintaining the structural integrity of GNPs throughout the procedure enhanced the mechanical and corrosion properties of the Mg-GNP composites. Their research illustrated that Mg-xGNPs with $x < 0.3$ wt.% may present potential biodegradable materials for implant applications. Moreover, more incorporation of GNPs, up to a specific amount, increased the mechanical properties of metal matrices including hardness and YS [121–123]. Nevertheless, throughout the composite fabrication procedure, structural modifications in dispersed GFNs take place such as re-agglomeration, with the following buildup of defects because of their connection with nearby GNPs in the agglomerate through friction and impact, which leads to the constantly changing mechanical and general performance of the Mg-based matrix [30]. A Mg-GNP composite was prepared via the SPM technique by Rashad et al. [91], and their results exhibited that GNP were actually dispersed uniformly in the Mg matrix and, for this reason, worked as a successful reinforcing phase to protect against further deformation. The enhancements in elongation (EL), $YS_{0.2\%}$, UTS, and Vickers HR were significantly higher for the Mg-0.3GNP composite in comparison with bare Mg. Rashad et al. [119] synthesized a Mg-1Cu-xGNP composite via the SPM technique, and their result showed that composite specimens presented higher mechanical strength compared to the bare Mg. The superior

strength of the composites might be caused by fundamental strengthening systems, such as CTE and EL mismatch, Orowan toughening, and stress transfer. In this context, Saberi et al. [110] synthesized a Mg-based-GNP composite through the SPM technique with various concentrations of GNPs. Their result presented that strong interfacial bonding was found between GNPs and the Mg-based alloy owing to the presence of residual oxygen in GNPs. Likewise, Yuan et al. [116] further confirmed that the existence of residual oxygen in GNPs had a critical role in increasing the interfacial bonding between the Mg matrix and reinforcement agent (GNPs). This great interfacial bonding resulted in increasing the mechanical characteristics including yield strength and elongation and the prevention of the occurrence of cavities at the Mg-Gr interface of the matrix and reinforcement agent (GNPs). This enhancement of the mechanical characteristics due to the presence of residual oxygen in GNPs was also found by Chen [90], Rashad [124], and Xiang et al. [83]. In another study, a Mg matrix encapsulated within 0.3 wt.% graphene via SSIT with the subsequent HTE procedure was demonstrated by Yang et al. [93]. Their result showed that the structure of the composite had been obviously refined after the HTE procedure, which resulted in the enhancement of the mechanical properties. The other reason for such strength improvement was related to the homogenous distribution of graphene and great interfacial bonding. The effect on the graphene family nanomaterials (GFNs) on the strength and ductility of the Mg-based alloy/composite is summarized in Table 2.

Table 2. Mechanical properties of Mg-based nanocomposites containing GFNs.

Samples	Processing route	E (GPa)	Tensile Performances			Compressive Performances			Hardness (HV)	Ref.
			0.2%TYS (MPa)	UTS (MPa)	Ductility or Elongation (%)	CYS (MPa)	UCS (MPa)	Failure Sstrain δ (%)		
Pure Mg	SPM	13.2 ± 0.3	187 ± 4	219 ± 5	3.45 ± 0.5	-	-	-	57.5 ± 2	[91]
Mg-0.3GNPs	SPM	14.6 ± 0.2	197 ± 3.1	238 ± 6	3.11 ± 0.4	-	-	-	68.5 ± 2	[91]
Mg-6Zn	DMD + Sintering + the	-	159 ± 5	276 ± 7	17 ± 1.5	109 ± 4.5	426 ± 6.1	21 ± 1.7	62.5	[91]
Mg-6Zn-0.5GNPs	DMD + Sintering + HTE	-	171 ± 4	295 ± 3.5	18 ± 1.9	226 ± 4.7	480 ± 5.6	20 ± 2	75	[100]
Mg-6Zn-1.5GNPs	DMD + Sintering + HTE	-	214 ± 2	313 ± 5.2	21 ± 1.1	226 ± 4.7	480 ± 5.6	16 ± 2.9	70	[100]
pure Mg	DMD + Sintering + HTE	-	96 ± 4	163 ± 3	7.5 ± 1.5	-	-	-	-	[99]
Mg-0.10 GNPs	DMD + Sintering + HTE	-	105 ± 1	176 ± 2	10.3 ± 0.6	-	-	-	-	[99]
Mg-0.25 GNPs	DMD + Sintering + HTE	-	122 ± 2	202 ± 3	14.5 ± 1.2	-	-	-	-	[99]
AZ31 alloy	PM + Sintering + Extrusion	-	195 ± 5	285 ± 2.9	14.5 ± 1.5	160 ± 6	363 ± 3.5	16.3 ± 1.5	58 ± 3	[125]
AZ31-0.3GNPs	PM + Sintering + Extrusion	-	173 ± 6.2	275 ± 5.7	21.7 ± 2.8	161 ± 4.5	397 ± 5.3	16.3 ± 1.5	71 ± 2.1	[125]
Pure Mg	SPM + Vacuum sintering + HTE	ET: 7.0 ± 0.3 EC: 6.4 ± 0.4	104 ± 4	164 ± 5	6.2±0.2	136 ± 3	286 ± 6	12 ± 0.2	46 ± 2	[111]
AZ31 Alloy	SC	-	183 ± 4.3	267 ± 6.5	9.74 ±1.5	100 ± 3.3	398 ± 5.1	21.0 ± 1.4	61	[126]
AZ31-1.5GNPs	SC	-	187 ± 3.5	284 ± 5.4	12.34 ± 3.4	121 ± 4.7	415 ± 3.4	21.2 ±2.1	65	[126]
AZ31-3GNPs	SC	-	195 ± 4.5	299 ± 6.2	12.56 ± 4.3	120 ± 2.8	406 ± 4.1	19.3±1.8	68.9	[126]
Mg-1Al	SPM + Vacuum sintering + HTE	ET: 12.8 ± 0.4 EC: 5.0 ± 0.3	155 ± 3	202 ± 3	6.9 ± 0.5	100 ± 2	377 ± 8	18 ± 0.5	50 ± 4	[111]
Mg-1Al-0.60 GNPs	SPM + Vacuum sintering + HTE	ET: 17.2 ± 0.1 EC: 7.6 ± 0.5	204 ± 9	265 ± 8		230 ± 5	407 ± 3	-	63 ± 2	[111]
Pure Mg	SPM + Vacuum sintering + HTE	ET: 7.4 ± 0.3 EC: 6.3 ± 0.4	104 ± 4	164 ± 5	6.2 ± 1.8	123 ± 5	264 ± 6	9 ± 2.5	40 ± 3	[119]
Mg-1Cu-0.18 Gr	SPM + Vacuum sintering + HTE	ET: 10.6 ± 0.4 EC: 5.9 ± 0.3	160 ± 6	240 ± 2	10.4 ± 2.1	140 ± 4	335 ± 8	-	44 ± 2	[119]
Mg-1Cu-0.36 Gr	SPM + Vacuum sintering + HTE	ET: 12.4 ± 0.25 EC: 8.4 ± 0.35	184 ± 3	252 ± 3	12.2 ± 1.3	143 ± 6	338 ± 5	-	46 ± 3	[119]
Mg-1Cu-0.54 Gr	SPM + Vacuum sintering + HTE	ET: 14 ± 0.16 EC: 7.7 ± 0.21	226 ± 5	260 ± 5	4.8 ± 2.5	166 ± 3	420 ± 6	-	56.7 ± 1	[119]
ZK60	SPM+ HTE + SC + HTE	-	158 ± 2.0	282 ± 3.0	11 ± 0.8	126 ± 3.0	364 ± 2.8	9 ± 0.3	68 ± 2.8	[92]
ZK60-0.05GNPs	SPM+ HTE + SC + HTE	-	256 ± 4.0	336 ± 4.0	13 ± 1.2	249 ± 4.0	473 ± 6.2	10 ± 1.0	78 ± 2.0	[92]
ZK60-0.1GNPs	SPM+ HTE + SC + HTE	-	283 ± 3.5	343 ± 3.8	17 ± 2.0	279 ± 3.4	463 ± 5.0	12 ± 1.1	75 ± 2.5	[92]
AZ61 Alloy	DMD + HTE	-	184 ± 5.5	300 ± 7.1	11.5 ± 1.9	170 ± 5.1	461 ± 6.8	16.7 ± 2.1	75.7 ± 2.5	[95]
AZ61-3GNPs	DMD + HTE	-	232 ± 4.9	335 ± 6.6	10.7 ± 2.1	226 ± 4.7	480 ± 5.6	15.1 ± 3.5	87.5 ± 1.8	[95]

Table 2. *Cont.*

Samples	Processing route	E (GPa)	Tensile Performances			Compressive Performances			Hardness (HV)	Ref.
			0.2%TYS (MPa)	UTS (MPa)	Ductility or Elongation (%)	CYS (MPa)	UCS (MPa)	Failure Sstrain δ (%)		
AZ80-0.5Ca	RC + Extrusion	-	104 ± 5.2	271 ± 13.5	4.4 ± 0.22	78 ± 3.9	340 ± 17	9.5 ± 0.33	71.3 ± 2	[127]
AZ80-0.5Ca-0.1GNP	RC + Extrusion	-	146 ± 7.3	310 ± 15.5	6.6 ± 0.33	90 ± 4.5	419 ± 21	13 ± 0.6	77.6 ± 2.6	[127]
AZ80-0.5Ca-0.6GNP	RC + Extrusion	-	160 ± 16	325 ± 32	9.3 ± 0.85	102 ± 10	361 ± 36	11.5 ± 0.7	88.9 ± 5	[127]
AZ31	-	-	215	256	13.3	-	-	-	56	[101]
AZ31-GNPs	FSP	-	217	278	15.8	-	-	-	79	[101]
AZ31-0.3Gr	MBM + HTE	-	214.82	310.79	5.99	-	-	-	-	[93]
Mg-0.3Sr-0.3Ca	SC + HTE	-	174	233	7.4	68	300	15.2		[114]
Mg-0.3Sr-0.3Ca-GNP	SC + HTE	-	213	235	10.2	90	303	16.9	55	[114]
Mg-0.3Sr-0.3Ca-GNPs + MgO	SC + HTE	-	224	239	13.8	96	330	18.3	68	[114]
Pure Mg	SPM + Vacuum sintering + HTE	-	162 ± 5	195 ± 4	3.7 ± 2.5	-	-	-	41 ± 4	[118]
Mg-0.5Al-0.18GNPs	SPM + Vacuum sintering + HTE	-	173 ± 4	230 ± 5.1	10.7 ±3	-	-	-	55 ± 2	[118]
Mg-1.0Al-0.18GNPs	SPM + Vacuum sintering + HTE	-	190 ± 5.3	254 ± 3	15.5 ± 3.4	-	-	-	58 ± 3.5	[118]
Mg-1.5Al-0.18GNPs	SPM + Vacuum sintering + HTE	-	209 ± 3.9	268 ± 4.5	12.7 ± 2	-	-	-	60 ± 3	[118]
Mg-1Al-1Sn	SPM + Extrusion	-	161 ± 04	236 ± 5.1	16.7 ± 03	-	-	-	-	[109]
Mg-1Al-1Sn-0.18GNPs	SPM + Extrusion	-	208 ± 5.3	269 ± 03	10.9 ± 3.4	-	-	-	-	[109]
Mg-0.3Sr-0.3Ca	SC + HTE	-	171 ± 8.5	228 ± 11.4	6 ± 0.3	65 ± 3.2	339 ± 17	14.3 ± 0.7	-	[96]
Mg-0.3Sr-0.3Ca-0.1GNP	SC + HTE	-	184 ± 9.2	232 ± 11	8.1 ± 0.4	67 ± 3.4	335 ± 16	15.5 ± 0.8	-	[96]
Mg-0.3Sr-0.3Ca-0.2GNPs	SC+ HTE	-	210 ± 10.5	231 ± 11.5	10 ± 0.5	93 ± 4.7	339 ± 18	18.3 ± 0.95	-	[96]
Mg-0.3Sr-0.3Ca-0.4GNPs	SC + HTE	-	223 ± 13.5	245 ± 15	8.8 ± 0.55	82 ± 5	309 ± 17	14.3 ± 0.9	-	[96]
AZ91-0.25GNPs	SPM	-	116 ± 9	172 ± 10	3.4 ± 0.7	-	-	-	65 ± 1.5	[117]
AZ91-0.50GNPs	SPM	-	128 ± 13	190 ± 14	2.8 ± 0.9	-	-	-	69 ± 2.5	[117]
Mg	SPM + Sintering + HTE	5.98	119 ± 5	186 ± 6	9.7 ± 3	-	-	-	41 ± 3.5	[120]
Mg-1Al-0.09GNPs	SPM + Sintering + HTE	13.40	148 ± 3	206 ± 4	10.5 ± 3.4	-	-	-	48 ± 2.9	[120]
Mg-1Al-0.18GNPs	SPM + Sintering + HTE	12.18	162 ± 4.1	223 ± 5	15.2 ± 2	-	-	-	51 ± 3	[120]
Mg-1Al-0.30GNPs	SPM + Sintering + HTE	13.84	178 ± 2.9	246 ± 3.5	16.9 ± 3	-	-	-	55 ± 4	[120]
Mg-10Ti	SPM + Extrusion	-	141 ± 04	212 ± 5.1	11 ± 03	-	-	-		[128]
Mg-10Ti-0.18 GNPs	SPM + Extrusion	-	160 ± 5.3	230 ± 03	14 ± 3.4	-	-	-		[128]
AZ91	SPM + HTE	-	168 ± 5.0	215 ± 6.0	7.0 ± 0.2	-	-	-	72.4 ± 2.0	[116]
AZ91-0.1GNPs	SPM + HTE	-	223 ± 3.6	276 ± 4.2	7.0 ± 0.2	-	-	-	78.2 ± 1.5	[116]

Table 2. *Cont.*

Samples	Processing route	E (GPa)	Tensile Performances			Compressive Performances			Hardness (HV)	Ref.
			0.2%TYS (MPa)	UTS (MPa)	Ductility or Elongation (%)	CYS (MPa)	UCS (MPa)	Failure Sstrain δ (%)		
AZ91-0.3GNPs	SPM + HTE	-	268 ± 4.6	318 ± 5.0	8.2 ± 0.1	-	-	-	84.4 ± 1.2	[116]
AZ91-0.5GNPs	SPM + HTE	-	296 ± 3.7	335 ± 4.8	8.2 ± 0.1	-	-	-	88.5 ± 1.0	[116]
AZ91-0.8GNPs	SPM + HTE	-	252 ± 5.5	307 ± 5.0	6.8 ± 0.1	-	-	-	81.6 ± 1.4	[116]
AZ91-1.2GNPs	SPM + HTE	-	TYS: 234 ± 3.0	287 ± 5.0	6.5 ± 0.2	-	-	-	74.7 ± 1.2	[116]
Mg-0.25GNPs	Sprayed GNPs on Mg foils (laminated composite) + HTE + Rolling	-	-	160	4.9	-	-	-	-	[115]
Mg-0.75GNPs	Sprayed GNPs on Mg foils (laminated composite) + HTE + Rolling	-	-	179	2.7	-	-	-	-	[115]
ZK60	Mechanical agitation + SC + HTE		161	281	15.6	-	-	-	-	[98]
ZK60-1GNPs	Mechanical agitation + SC + HTE	-	261	336	16.6	-	-	-	-	[98]
Mg-6Zn	In situ reaction wetting process + SC + HTE procedure	46.9 ± 0.7	136 ± 5	269 ± 6	19.5 ± 2.0	-	-	-	-	[97]
Mg-6Zn-0.1(GO-ZnO)	In situ reaction wetting process + SC + HTE	47.4 ± 0.3	206 ± 2	306 ± 5	15.1	-	-	-	71 ± 2.9	[97]
Mg-6Zn-0.3(GO-ZnO)	In situ reaction wetting process + SC + THE	47.8 ± 0.5	221 ± 4	316 ± 3	14.8	-	-	-	86 ± 3.6	[97]
Mg-3Zn-1Ca	SPM	-	-	-	-	-	8559 N	-	48	[110]
Mg-3Zn-1Ca-0.5GNP	SPM	-	-	-	-	-	14,900 N	-	57	[110]
Mg-3Zn-1Ca-1GNPs	SPM	-	-	-	-	-	20,586 N		60	[110]
Mg-3Zn-1Ca-2GNPs	SPM	-	-	-	-	-	2002 N		62	[110]
Pure Mg	HEBM + Compaction + Sintering	-	-	-	-	59 ± 2	85 ± 10	6 ± 0.5	-	[30]
Mg-0.1GNP Particle size (15 μm)	HEBM + Compaction + Sintering	-	-	-	-	99 ± 1	146 ± 5	12 ± 2.4	-	[30]
Mg-0.2GNP Particle size (15 μm)	HEBM + Compaction + Sintering	-	-	-	-	130 ± 4	182 ± 14	6 ± 3.9	-	[30]
Mg-0.3GNP Particle size (15 μm)	HEBM + Compaction + Sintering	-	-	-	-	126 ± 6	246 ± 1	14 ± 1.7	-	[30]
Mg-0.1GNP Particle size (5 μm)	HEBM + Compaction + Sintering	-	-	-	-	76 ± 5	143 ± 14	9 ± 0.3	-	[30]
Mg-0.2GNP Particle size (5 μm)	HEBM + Compaction + Sintering	-	-	-	-	97 ± 6	183 ± 4	13 ± 0.2	-	[30]

Table 2. *Cont.*

Samples	Processing route	E (GPa)	Tensile Performances			Compressive Performances			Hardness (HV)	Ref.
			0.2%TYS (MPa)	UTS (MPa)	Ductility or Elongation (%)	CYS (MPa)	UCS (MPa)	Failure Sstrain δ (%)		
Mg-0.3GNP Particle size (5 μm)	HEBM + Compaction + Sintering	-	-	-	-	110 ± 8	169 ± 18	9 ± 0.8	-	[30]
AZ61-0.2GO	SPM + SLM	-	-	-	-	~177.5	-	-	93	[102]
AZ61-0.4GO	SPM + SLM	-	-	-	-	~188.5	-	-	97	[102]
AZ61-0.6GO	SPM + SLM	-	-	-	-	~202.5	-	-	100	[102]
AZ61-0.8GO	SPM + SLM	-	-	-	-	~208.75	-	-	102	[102]
AZ61-1GO	SPM + SLM	-	-	-	-	~221.05	-	-	104.5	[102]
AZ61-1.2GO	SPM + SLM	-	-	-	-	~192.5	-	-	108.52	[102]

GNPs: graphene nanoplatelets, DMD: disintegrated melt deposition, PM: powder metallurgy, SPM: semi-powder metallurgy, HTE: hot extrusion, SC: stir casting, HEBM: high energy ball milling, MBM: mechanical ball milling, SLM: selective laser melting, RC: rheocasting, E: elastic modulus, ET: elastic modulus in tensile, EC: elastic modulus in compressive, TYS: tensile yield strength, UTS: ultimate tensile strength, CYS: compressive yield strength, UCS: ultimate compressive strength.

7. Biocorrosion and Biodegradability of Mg-GFNs-Based Composites

The entire biomaterial should make it through a certain healing period for 12–18 weeks [14,125–128]. All examinations regarding Mg-based alloys have demonstrated high degradation, where the Mg alloys are fully absorbed prior to the least healing duration of 12 weeks [129], which results in H_2 gas release, inducing cavities, reduced mechanical integrity, regional swelling, and discomfort for the patient [130–132]. To address this restriction, Mg-based composites that were recently fabricated intended for implant applications should possess corrosion rates lower than 0.5 mm/year in physiological fluids at 37 °C [133]. The corrosion mechanism can be understood by analyzing the corroded surfaces of Mg-based specimens when exposed to the SBF. As can be seen in Figure 13, Mg-based specimens react with the SBF along with H_2 generation. The general corrosion reaction of Mg in physiological media is presented below [134]:

$$Mg + 2H_2O \rightarrow Mg(OH)_2 + H_2\uparrow \quad (1)$$

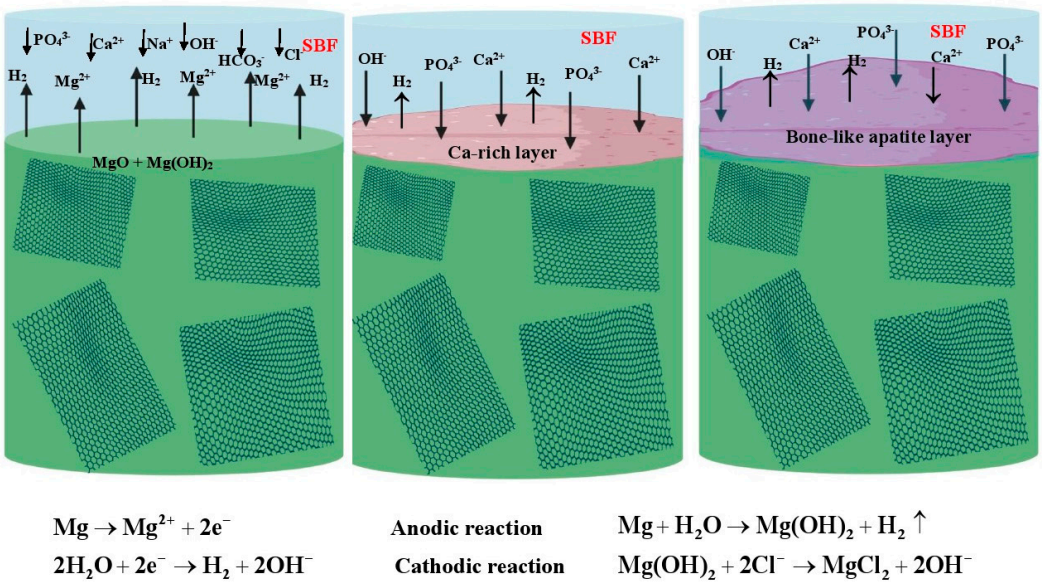

Figure 13. Schematic diagram for the corrosion product deposition on the surface of Mg-based specimens when exposed to the SBF.

Based on the previously mentioned reactions, $Mg(OH)_2$ is created on the Mg alloy surface. The chloride ion is considered to have an adverse effect on the corrosion resistance of Mg. Numerous investigations have verified that a high chloride amount is facilitated by replacing $Mg(OH)_2$ with $MgCl_2$ and enhances the degradation rate of the Mg alloy [135]. On the other side, the OH^- coming initially from Mg degradation can easily react with the HPO_4^{2-} in physiological fluids based on Equation (2), leading to the generation of PO_4^{3-}.

$$HPO_4^{2-} + OH^- \rightarrow PO_4^{3-} + H_2O \quad (2)$$

Subsequently, the PO_4^{3-} reacts with the Ca^{2+} in physiological media or Mg^{2+} to deposit apatite or Mg-P on the composite surface [136–139]. Phosphate ions might slow down the corrosion rate significantly and postpone the occurrence of pitting corrosion [135]. Neupane et al. [140] suggested the increased corrosion resistance of GNPs embedded within the Mg matrix. GNPs were successfully embedded into nanocomposites, which led to augmenting new bone generation and restoration because GNPs tend not to simply degrade in physiological fluids and anti-infiltrate corrosive media, thus reducing the degradation rate of the Mg-based composite [133]. A Similar examination showed

that [138–140] the corrosion performance of Mg-based composites was enhanced by the embedding of sufficient amounts of GFNs.

Shuaia et al. [102] fabricated a Mg alloy/GO composite with a 3D honeycomb nanostructure accompanied by remarkable corrosion resistance via the SLM process. Outcomes revealed that GO dispersed along the GBs and progressively covered α-Mg grains as the GO amount increased. Because of this remarkable anti-infiltration property of GO, the honeycomb nanostructure served as a solid obstacle to inhibit the increasing corrosion rate. The oxygen-incorporating groups on GO accelerate the precipitation of apatite and additionally inhibit further attack of the corrosive solution [141,142]. Turan et al. [107] also prepared Mg-xGNPs (x = 0.1, 0.25, and 0.5 wt.%) composites via SPM approaches with GNPs. A homogeneous dispersion was attained for the entire specimens while partial agglomeration might be observed in Mg-0.5GNPs. In comparison with the bare Mg, the corrosion property was impacted adversely in composite encapsulated within graphene. In this context, Rashad et al. [143] likewise examined the influence NaCl solutions have on the corrosion performance of Mg-Gr composites. The outcomes showed that the existence of GNPs in various matrices reduces the corrosion property of the composites. They also revealed that due to the presence of dislocation amounts at the interface of composites, crevice invasions were generated, and hence, GNPs induce the corrosion of Mg/Mg alloys as a result of the galvanic cell; this particular effect increases with increasing GNP amount. The corrosion rates with various processing methods, corrosion solutions, and measurement techniques are described in Table 3.

Table 3. Corrosion properties of Mg-based nanocomposite containing GFNs.

Samples	Reinforcement	Processing Route	Reinforcement Particle Size	Corrosion Medium	Icorr ($\mu A.cm^{-2}$)	Ecorr vs. SCE	Corrosion Rate (mm/year)			Rp ($\Omega.cm^2$)	Ref
							Non Polarized		Polarized		
							Immersion Time (h)	HE or WL	PDP		
Pure Mg	-	HEBM + Compaction+ Sintering	-	Hank's	0.81 ± 0.02 ($mA.cm^{-2}$)	-	24	32.52 ± 1.58 $mL.cm^{-2}.day^{-1}$ 74.11 ± 3.61 mm/year	25.02 ± 1.79		[30]
Mg	0.1GNPs		Particle size (15 µm); thickness (5 nm)		0.42 ± 0.02 ($mA.cm^{-2}$)	-		15.16 ± 0.41 $mL.cm^{-2}.day^{-1}$ 34.57 ± 0.94 mm/year	13.28 ± 0.27	-	
	0.2GNPs				0.58 ± 0.03 ($mA.cm^{-2}$)	-		26.93 ±1.08 $mL.cm^{-2}.day^{-1}$ 61.38 ± 2.48 mm/year	18.50 ± 0.83	-	
	0.3GNPs				0.35 ± 0.04 ($mA.cm^{-2}$)	-		30.41 ± 1.39 $mL.cm^{-2}.day^{-1}$ 69.32 ± 3.16 mm/year	11.00 ± 1.08	-	
Mg	0.1GNPs		Particle size (5 µm); thickness (9 nm)		0.50 ± 0.05 ($mA.cm^{-2}$)	-		29.55 ± 2.61 $mL.cm^{-2}.day^{-1}$ 67.35 ± 5.95 mm/year	15.13 ± 0.91	-	
	0.2GNPs				0.69 ± 0.03 ($mA.cm^{-2}$)	-		31.54 ± 2.97 $mL.cm^{-2}.day^{-1}$ 71.88 ± 6.77 mm/year	21.45 ± 1.91	-	
	0.3GNPs				0.91 ± 0.03 ($mA.cm^{-2}$)	-		34.93 ± 1.82 $mL.cm^{-2}.day^{-1}$ 79.62 ± 4.17 mm/year	28.74 ± 3.06	-	
Mg-Sr-Ca	-	SC + HTE	-	SBF	7.373	1.832	-	-	0.241		[114]
Mg-Sr-Ca	GNPs	SC + HTE	-		6.980	1.776	-	-	0.231	-	
Mg-Sr-Ca	GNPs + MgO	SC + HTE	-		9.279	1.800	-	-	0.269	-	
AZ61	-	SPM + SLM	-	SBF	50 ± 4	1.54 ± 0.02	360	-	1.21 ± 0.09	-	[102]
AZ61	0.2GO		Diameter (8–15 µm)		89 ± 12	1.54 ± 0.02			2.03 ± 0.27	-	
	0.4GO				212 ± 16	1.52 ± 0.03		205.23 $mL.cm^{-2}$	4.84 ± 0.36	-	
	0.6GO				118 ± 13	1.57 ± 0.02			2.67 ± 0.30	-	

Table 3. *Cont.*

Samples	Reinforcement	Processing Route	Reinforcement Particle Size	Corrosion Medium	Icorr ($\mu A.cm^{-2}$)	Ecorr vs. SCE	Corrosion Rate (mm/year)			Rp ($\Omega.cm^2$)	Ref
							Non Polarized		Polarized		
							Immersion Time (h)	HE or WL	PDP		
	0.8GO				85 ± 6	1.51 ± 0.02			1.94 ± 0.14	-	
	1.0GO				35 ± 3	1.56 ± 0.03		15.3 $mL.cm^{-2}$	0.76 ± 0.07	-	
	1.2GO				135 ± 15	1.53 ± 0.02		65.25 $mL.cm^{-2}$	3.08 ± 0.34	-	
AZ31	-	SPM	-	0.1 M Na2SO4	371.54	1.416	-	-	~4	108.6 (Ω)	[143]
AZ31	0.2r-GO		Thickness (up to 5.8 nm)		992.08	1.456	-	-	~11.5	465.7 (Ω)	
	0.3r-GO				207.25	1.464	-	-	~2.4	755 (Ω)	
	0.4r-GO				61.21	1.328	-	-	~0.5	221.4 (Ω)	
	0.5r-GO				207.41	1.464	-	-	~1.8	754 (Ω)	
Mg-3Zn-Ca	0.5GNPs	SPM	-	SBF	186.54	1.46	-	-	-	134.57	[110]
	1GNPs		-		112.89	1.45	-	-	-	166.55	
	2GNPs		-		420.76	1.49	-	-	-	66. 21	
AZ91	GNPs	SPM	Diameter (5, 8 nm); surface area (about 750 m^2/g)	3.5 wt.% NaCl	388.43 µA	1.491	-	-	4.92	-	[108]
AZ31	-	SC	Diameter (5, 8 nm); surface area (about 750 m^2/g)	3.5 wt.% NaCl	15.47 µA	1.453	-	-	-	-	[141]
AZ31	1.5GNPs				18.13 µA	1.465	-	-	-	-	
AZ31	3.0GNPs				19.31 µA	1.479	-	-	-	-	
AZ61	-				11.54 µA	1.457	-	-	-	-	
AZ61	3.0GNPs				14.21 µA	1.476	-	-	-	-	
Pure Mg	-	SPM	-	-	0.12 ($mA.cm^{-2}$)	1.63	-	-	249.9 (mpy)	-	[107]
Mg	0.1 GNPs		Thickness (5–8 nm); surface area (750 m^2/g)	3.5 wt.% NaCl	0.51 ($mA.cm^{-2}$)	1.59	-	-	1048 (mpy)	-	
	0.25 GNPs				0.89 ($mA.cm^{-2}$)	1.58	-	-	1813 (mpy)	-	
	0.50 GNPs				1.02 ($mA.cm^{-2}$)	1.59	-	-	2090 (mpy)	-	
Mg-0.5 MWCNT	GNPs	PEO Coating	-	3.5 wt.% NaCl	101 µA	1.424	-	-	14.46 (mpy)	-	[144]

GNPs: graphene nanoplatelets, MWCNTs: multi-walled carbon nanotubes, I_{corr}: corrosion current density, E_{corr}: corrosion potentials, HE: hydrogen evolution, WL: weight loss, PDP: potentio-dynamic polarization, Rp: polarization resistance, DMD: disintegrated melt deposition, PM: powder metallurgy, SPM: semi-powder metallurgy, HTE: hot extrusion, SC: stir casting, HEBM: high energy ball milling, SLM: selective laser melting, PEO: plasma electrolytic oxidation.

8. Biodegradability of Mg-GFN-Based Composites

Commonly, GNPs tend not to simply degrade in physiological fluids; even so, their full degradation might be attained by human enzymes accelerating chemical reactions in the body [137]. GNPs offer a distinctive orientation of sp^2 carbon atoms, creating a 2D structure (honeycomb shape) with great electron density, ultimately causing an impenetrable performance against entire gas molecules, which increase the corrosion resistance of Mg alloys [47,144–147]. The GNPs with a thin layer work as a barrier film within the metal matrix, leading to a substantial lessening in current densities and subsequent corrosion rates throughout immersion tests of composites containing GNPs [138,139]. GNPs, by possessing an atomic-scale barrier, are also favorable in reducing or suppressing H_2 gas formation in Mg-based specimens during the degradation process when exposed to the body fluids, as presented in Figure 14 [47].

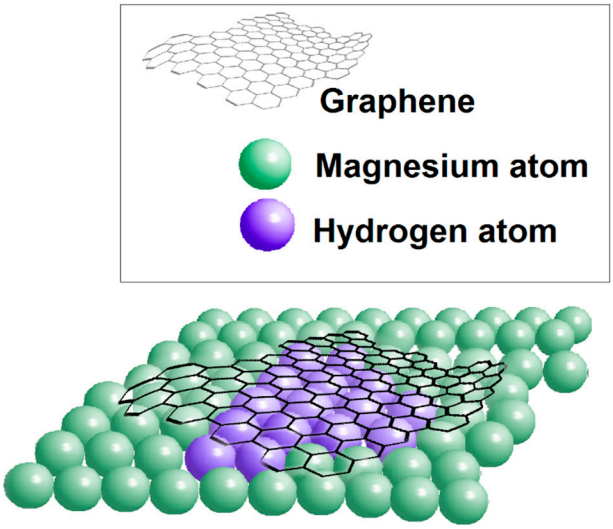

Figure 14. Schematic illustration of the inhibition of hydrogen gas release via the atomic-scale barrier of a graphene sheet on the in vivo degradation of Mg-based implants, reproduced from [47], with permission from Wiley, 2019.

Neupane et al. [140] revealed the improved anti-corrosion behavior of GNPs embedded in Mg substrates. The impenetrability and outstanding mechanical characteristics (1100 GPa) of GNPs make them suitable as an additive phase (reinforcement agent) embedded into the Mg matrix for implant applications. As mentioned previously, the degradation of GNPs mostly takes place in enzymatic oxidation in biological fluid [148], while surface treatment of GNPs results in the attachment of specific FGs including carboxylic acid, which is favorable for degradation performance. The great specific surface areas of GNPs additionally help their degradation behavior by improving the biomolecules' attraction on the surfaces [149]. Other researchers also further confirmed that these elements likewise have an effect on the degradation process of GNPs including 2D planar sheets that offer substantially more connection surfaces with the biomolecules [150], along with the unsmooth, wrinkled surface morphology of GNPs, noticeably promoting their interlocking performance with the surrounding media, hence improving the attachment of biomolecules on their surfaces [151]. It should be mentioned that the volume fraction of GNPs in metal-based biomaterials ought to be in the amount of 1–10% due to the fact that a high concentration of GNPs results in dramatically elevated stiffness of the composite, which would possibly not be biomechanically suitable with natural bone.

9. Cellular Response of Mg-GFN-Based Composites

Regardless of the appealing features of MMNCs incorporating different nano-additive phases, safety and toxicity issues hinder their use in bone tissue engineering (BTE). The most recent

advancements in nanotechnology have made it possible for experts to create composite materials presenting appealing characteristics by modulating their features on the nanoscale. Nevertheless, from the viewpoint of biomedical purposes, biological characteristics and the interaction of these nanomaterials in an SBF have remained questionable subjects as a result of unclear studies on their toxicity. For that reason, it is crucial to further examine the biological characteristics of these composites including cell response, biocorrosion, and cytotoxicity. Biodegradable materials including Mg absorb in vivo and dissolve fully after fulfilling the healing process time. The alloying elements are the key factors of biodegradable materials that might be effortlessly absorbed by the body. Nevertheless, Mg-based composites degrade quickly in physiological media prior to adequate healing of the tissues. This kind of quick degradation of Mg-based composites likewise affects their capacity to be used for load-bearing implant purposes [152]. Typically, the biocompatibility of MMNCs is determined by their connections with different biological systems including cells, proteins, and other complex biomolecules, for example DNA [152]. It is actually recognized that GFNs cause the attachment of cell-binding proteins and the following cellular attachment [153,154]. The effective binding of proteins existing in SBF and tissues on the GFNs results in the generation of biocorona protein on composite surfaces [155]. The structure of this kind of biocorona primarily relies on the intrinsic characteristics of Gr and has the ability of modifying of the extracellular matrix (ECM). Consequently, the tendencies of Gr in biological systems are usually accurately forecasted by knowing the creation procedure of biocorona on their surfaces [47,154]. Current reports likewise revealed that π-π stacking, a result of the solid van der Waals force, is actually identified as a dominant adsorption system of proteins on top of the GNPs' surfaces. This kind of solid π-π stacking mainly takes place among the solid sp^2 bonding of carbon atoms in GFNs and the benzene rings in amino acids [156,157]. Accordingly, any kind of enzymatic degradation of GNPs through the defense mechanisms of competent cells could work as a distinctive case of biocoronal interactions within the body. GNP embedded nanocomposites are effective in electrically inducing tissues owing to their outstanding conductive characteristics, and this is favorable in facilitating new bone generation and restoration. These sorts of conductive nanobiomaterials likewise enhance the adsorption of ECM proteins, hence enhancing the expression of osteogenic differentiation and the generation of pertinent growth factors. BMP is a widely recognized protein that elevates the osteogenic differentiation of Mg-based composites containing GFNs and has demonstrated outstanding attachment on the Gr surfaces [154,156,157]. In this regard, it was suggested [34] that the bacterial cytotoxicity of GFNs could possibly be caused by both membrane and oxidative stress. GFNs have a tendency to lead to cellular attachment, due to the fact that it really is more probable to interact with bacterial cells because of the greater density of FGs and small size [35]. GFNs could destroy the cells as a result of membrane stress generation, which results in destroying the cell walls [34]. This sort of biocompatibility causes this to be an appealing nano-additive phase for MMNCs. In vitro cytotoxicity examinations were performed by Saberi et al. [110] and Munir et al. [30], and no negative consequences with encapsulation of GNPs in pure Mg and Mg-based matrix, respectively, were found. Mg-based matrix with homogeneously distributed GNPs with lower defect amounts presented a greater level of cell viability ratio (CVR). Furthermore, MG-63 cells were observed by Shuai et al. [102] to be attached and to greatly proliferate on AZ61-1.0GO alloy and exhibited greater cytocompatibility as opposed to AZ61 alloy. The sluggish corrosion along with lower pH value increase cause greater cell attachment and growth on the nanocomposite surface with a lower content of GNPs [110]. Nevertheless, Saberi et al. [110] exhibited that more addition of GNPs up to 2 wt.% had an effect on cellular attachments and diminished the density and growth of the cells resulting from activating the mitochondrial pathway. Table 4 exhibits in vitro the cytotoxicity examination regarding Mg-GFN composites.

Table 4. The cellular characterization in Mg-GFN-based nanocomposites.

Materials	Processing Route	Reinforcement Particle Size	Cell Type	Cell Viability (%)	ALP Activity	Cell Attachment	Application	Ref.
Mg-0.1GNPs	HEBM + PM	Particle size (15 μm); thickness (5 nm)	SaOS-2 cells	CVR: 1.13	-	Excellent	In vitro	[30]
Mg-0.2GNPs	HEBM + PM	Particle size (15 μm); thickness (5 nm)	SaOS-2 cells	CVR: 0.92	-	Excellent	In vitro	[30]
Mg-0.3GNPs	HEBM + PM	Particle size (15 μm); thickness (5 nm)	SaOS-2 cells	CVR: 0.9	-	Excellent	In vitro	[30]
AZ61-1GO	SPM + SLM	Diameter (8–15 μm)	MG-63 cells	Optic density = 1.7 after 5 days	-	Good	In vitro	[30]
Mg-3Zn-Ca-0.5GNPs	SPM	-	MG-63 cells	83 % for 24 h 87 % for 48 h	3.4 for 24 h 4.7 for 48 h	Adequate	In vitro	[102]
Mg-3Zn-Ca-1GNPs	SPM	-	MG-63 cells	65 % for 24 h 60 % for 48 h	3.7 for 24 h 5.5 for 48 h	Adequate	In vitro	[110]
Mg-3Zn-Ca-2GNPs	SPM	-	MG-63 cells	100 % for 24 h 100 % for 48 h	2.5for 24 h 3.4 for 48 h	Adequate	In vitro	[110]
Mg-1ND	PM	Particle size < 10 nm	L-929 cells	93.2 % for 24 h 105.8 % for 72 h	-	Good	In vitro	[110]
Mg-3ND	PM	Particle size < 10 nm	L-929 cells	94.1 % for 24 h 102.2 % for 72 h	-	Good	In vitro	[158]
Mg-5ND	PM	Particle size < 10 nm	L-929 cells	95.4 % for 24 h 113.1 % for 72 h	-	Good	In vitro	[158]

* HEBM: high energy ball milling, PM: powder metallurgy, SPM: semi-powder metallurgy, SLM: selective laser melting, ND: nanodiamond, CVR: cell viability ratio.

10. Antibacterial Performance of Mg-GFN-Based Composites

Saberi et al. [110] demonstrated that Mg-GNP composites offered great antibacterial performance towards Gram-positive (*S. aureus*) and Gram-negative (*E. coli*) bacteria based on disk diffusion. According to the results, employing GNPs within the Mg matrix improves the inhibition zone. The charge transfers and the infiltration into the cells are the primary antibacterial systems [34,159]. As soon as the bacterial cells come into contact with the GFNs, they will likely be finally damaged as a consequence of numerous mechanisms including membrane stress, oxidative stress, and/or wrapping isolation. The bacterial development is prevented through these mechanisms that might function independently or with each other [160]. Initially, the bacterial cells were resistant to the Gr-based materials for a limited period, and subsequently, owing to a few cells having a smaller weight of surface phospholipid, the cell walls' integrity was to some extent sacrificed. Ultimately, an extreme reduction happened in the cell walls [160]. Within these conditions, the lipid bilayer is infiltrated by coming into contact with the GNPs. The membrane layer is routinely pierced by the sharp sheet edges of the GFNs, which reduce the energy required for membrane infiltration. Among the elements that could assist in the cell membrane layer destruction are the negative charges of the bacterial cells, which enhance the connections with the sheet edges, since they function as great electron acceptors.

It is suggested that the primary function of oxidative stress is the antibacterial activity of GO. Actually, the oxidation of lipids, nucleic acids, and proteins that ultimately contributes to cell membrane layer damage and cellular growth inhibition is caused by the activity of oxidative stress on bacteria [34]. The reactive oxygen species' (ROS) release is the reason for this inhibition that might result in the modification of the cellular redox circumstance. In the condition in which usually the particles are absorbed, the main systems for cellular protection are generally oxidative stress, as well as ROS release. By disturbing the equilibrium among the intracellular oxidant and antioxidant functions, the GNPs might enhance the oxidative stress [161]. The ROS, which usually can destroy cellular parts, in particular proteins and DNA, commonly includes OH, O^{2-}, and H_2O_2 [162]. Following that, Gr exhibited antibacterial capacity, despite the fact that GO of similar amounts showed greater antibacterial performance than that of Gr. The main antimicrobial mechanisms were charge transfer and infiltration into the cell walls [163]. Consequently, Gr and GO with their antimicrobial capacity might fulfill the specifications regarding bone restoration components below the safety limit [161]. Another investigation [159] demonstrated that Gr seriously destroys and deactivates the microorganisms when it attaches to them. This antimicrobial action was effective and quick against *E. coli* and *S. aureus*, and the destruction took place mainly in the cell membrane layer. Based on an examination, the Gr nanosheets experienced a greater antimicrobial capacity than standard antibiotics including kanamycin. Likewise, concerning the antimicrobial mechanisms, Shuai et al. [164] revealed that the inhibitory characteristics of the Gr-based nanocomposites elevated cellular injuries owing to the occurrence of oxidative stress. In other research [163], GFNs, for instance fullerene and CNTs, were considered as the agents to generate the oxidative stress. Furthermore, consistent with some other examinations, the cell wall experiences a charge imbalance, which might destroy the cell walls. The solid connection of the negatively charged microbial cell walls with the outstanding electron acceptors Gr encapsulated nanocomposites results in the previously mentioned electrons from the bacterial membrane to the GNPs, and therefore, the microbial cell walls might be encircled by means of a conductive system. For that reason, this destroys the microbial cell by way of generating oxidative stress in the microbial cell membrane.

11. Future research Directions in using GFNs for Bone Tissue Engineering

The potential of Mg-based encapsulated GFNs was reviewed in the former sections, suggesting their use as new biomaterials pertaining to BTE. All of the research indicated that GFNs are appearing as new components in the associated areas of biomedicine, drug release systems, and TE, and they are developing quickly. Comprehensive investigation is continuing to set up a system for employing GFNs as the nano-additive phase in present metallic biomaterials to be able to create new and very

useful implants and scaffolds for TE usage. For these kinds of nanocomposites, a lower amount of CNT and Gr (≈ 5 vol.%) was recommended, thus to restrict the portions getting into the human body system [165]. The immobilization of CNT and Gr in metallic biomaterials prevents the exposure of adjacent tissues, therefore providing biosafety for these kinds of particles [47]. It is worth noting that the application of biodegradable Mg-GFN composites fabricated through various fabrication procedures and structural modifications for load-bearing implant process for bone substitution and reproduction attracts a huge amount of attention [166–180]. Taking into consideration the outstanding biological response and incredible mechanical characteristics of Gr, as described in earlier sections, it is anticipated that a number of implants and scaffolds will be created in the near future. Despite the fact that the results from initial in vitro and in vivo biological tests on Gr are motivating, additional comprehensive, methodical research works are expected to comprehend their long-term biological results. With the current literature on the biomedical usage of Gr, it is still not feasible to determine them as safe components concerning BTE. Among the key factors for the inability of these nanomaterials to convert directly into clinically verified use is the absence of reliable in vivo research to evaluate their nanotoxicity. In addition to other biomedical usage, GFN-based implants and scaffolds for BTE are usually regarded as safe as there is minimal chance that these nano-additive phases in metal matrices are going to be directly connected to living microorganisms. These demands create mindful technology and scientific strategies to reduce the nanotoxicological effect of Gr even while keeping the appealing ideal characteristics regarding BTE. The current review article offers more examination to be performed to utilize GFNs as nano-additive phases for Mg-based alloys. Specifically, additional in vivo examination is required to confirm the appropriateness of these materials for implant usage.

12. Conclusions

This review significantly examined the possibilities, current progress, challenges, and upcoming exploration guidelines with regard to GFNs as nano-additives (reinforcements) in Mg-based matrices. Mg alloys have benefits compared to the traditional stainless steel, Co-based alloys, and Ti-based alloys because of the outstanding biodegradability and cytocompatibility along with the appropriate mechanical performance concerning implant usage [181–202]. From this perspective, the mechanical characteristics of bioimplants ought to be adequate to maintain their strength throughout the healing process. Nano-additives (reinforcements) are able to enhance the mechanical integrity of Mg-based composites along with ductility at the same time. Following that, GFNs effectivity act as functional components and reinforcement phases for Mg-based composites, which offer distinctive characteristics including large surface areas and outstanding mechanical, thermal, and electrical characteristics, along with great chemical stability. The synergetic capability of GFNs to enhance ductility together with strengthening, as well as decreasing weight is extremely attractive and prevails over the drawbacks of other reinforcement phases like ceramic particles. Furthermore, GFNs, in particular GO, have considerable biological characteristics and reveal effective antibacterial performance owing to ROS release and oxidative stress. Furthermore, the fabrication process of composites such as SC, PM, SPM, SLM, and FSP, as well as other parameters including GFN amount and type have a significant effect on the mechanical, anticorrosion, and biological properties Mg-based composites encapsulated within GFNs. On top of that, apparently, the presence of GFNs, in particular GO and GNPs, within Mg-based matrices in lower amounts could provide better anticorrosion and biological properties in vitro and in vivo. In addition, there are widely recognized strengthening systems for Mg matrices; among them, refined grain structure, Orowan looping, and stress transfer are the primary strengthening mechanisms in Mg matrices strengthened by GNPs. Taken together, GFNs as nano-additive phases (reinforcement agents) offer incredible potential to be employed for load-bearing implants and BTE applications. However, the cytocompatibility of GFNs is nevertheless an arguable matter that hinders developments in employing these appealing reinforcement agents for clinical usage. Their safe clinical implementation as revolutionary reinforcement agents for application in load-bearing implants and BTE requires additional assessment.

Author Contributions: Conceptualization, supervision, formal analysis, writing—review and editing, A.S.; H.R.B.-R., writing—review and editing, S.R.; writing—original draft preparation, methodology, formal analysis, S.A.; supervision, writing—review and editing, funding acquisition, F.B. All authors have read and agreed to the published version of the manuscript.

Funding: This research received no external funding.

Acknowledgments: The authors would like to thank the Norwegian University of Science and Technology, Islamic Azad University, Najafabad, and Amirkabir University on Technology for providing the facilities for this research.

Conflicts of Interest: The authors declare that they have no competing/financial conflict of interests in this paper.

Abbreviations

MMCs	Metal matrix composites
MMNCs	Metal matrix nanocomposites
GFNs	Graphene family nanomaterials
Gr	Graphene
GNPs	Graphene nanoplatelets
GO	Graphene oxide
rGO	Reduced graphene oxide
GRO	Graphite oxide
CNTs	Carbon nanotubes
MWCNTs	Multi-walled carbon nanotubes
SBF	Simulated body fluid
GB	Grain boundary
CMG	Chemically modified graphene
BG	Bioglass
PM	Powder metallurgy
DMD	Disintegrated melt deposition
MSDR	Multi-step dispersion route
SPM	Semi-powder metallurgy
HTE	Hot extrusion
SC	Stir casting
HEBM	High energy ball milling
MBM	Mechanical ball milling
SLM	Selective laser melting
SSTS	Semi-solid treatment stirring
RC	Rheocasting
UTS	Ultimate tensile strength
TS	Tensile strength
TYS	Tensile yield strength
E	Elastic modulus
EL	Elongation
E_T	Elastic modulus in tensile
CS	Compressive strength
UCS	Ultimate compressive strength
E_C	Elastic modulus in compressive
CYS	Compressive yield strength
CTE	Coefficient of thermal expansion
FGs	Functional groups
CIP	Cold isostatic pressing
HP	Hot pressing
HIP	Hot isostatic pressing
SPS	Spark plasma sintering
HTE	Hot extrusion
HF	Hot forging

HR	Hot rolling
FSP	Friction stir processing
ECA	Equal channel angular processing
MA	Mechanical alloying
I_{corr}	Corrosion current density
E_{corr}	Corrosion potentials
HE	Hydrogen evolution
WL	Weight loss
PDP	Potentio-dynamic polarization
Rp	Polarization resistance
PEO	Plasma electrolytic oxidation
FSW	Friction stir welding
TE	Tissue engineering
BTE	Bone tissue engineering
CVR	Cell viability ratio
ECM	Extracellular matrix
ROS	Reactive oxygen species
BMP	Bone morphogenetic protein

References

1. Mullan, B. Annual Report-Australia. *Eur. Heal. Psychol.* **2015**, *17*, 214–215.
2. Han, H.-S.; Loffredo, S.; Jun, I.; Edwards, J.; Kim, Y.-C.; Seok, H.-K.; Witte, F.; Mantovani, D.; Glyn-Jones, S. Current status and outlook on the clinical translation of biodegradable Metals. *Mater. Today* **2019**, *23*, 57–71.
3. Li, N.; Zheng, Y. Novel magnesium alloys developed for biomedical application: A review. *J. Mater. Sci. Technol.* **2013**, *29*, 489–502. [CrossRef]
4. Zheng, Y.F.; Gu, X.N.; Witte, F. Biodegradable metals. *Mater. Sci. Eng. R.* **2014**, *77*, 1–34. [CrossRef]
5. Lee, J.-M.; Salvati, E.A.; Betts, F.; DiCarlo, E.F.; Doty, S.B.; Bullough, P.G. Size of metallic and polyethylene debris particles in failed cemented total hip replacements. *J. Bone Joint. Surg. Br.* **1992**, *74*, 380–384. [CrossRef]
6. Bakhsheshi-Rad, H.R.; Akbari, M.; Ismail, A.F.; Aziz, M.; Hadisi, Z.; Pagan, E.; Daroonparvar, M.; Chen, X. Coating biodegradable magnesium alloys with electrospun poly-L-lactic acid-åkermanite-doxycycline nanofibers for enhanced biocompatibility, antibacterial activity, and corrosion resistance. *Surf. Coat. Technol.* **2019**, *37*, 124898. [CrossRef]
7. Hermawan, H. Biodegradable metals: State of the art. In *Biodegradable Metals*; Springer: Berlin, Germany 2012; pp. 13–22.
8. Yun, Y.; Dong, Z.; Lee, N.; Liu, Y.; Xue, D.; Guo, X.; Kuhlmann, J.; Doepke, A.; Halsall, H.B.; Heineman, W.; et al. Revolutionizing biodegradable metals. *Mater. Today* **2009**, *12*, 22–32. [CrossRef]
9. Moravej, M.; Mantovani, D. Biodegradable metals for cardiovascular stent application: Interests and new opportunities. *Int. J. Mol. Sci.* **2011**, *12*, 4250–4270. [CrossRef]
10. Gong, H.; Agustin, J.; Wootton, D.; Zhou, J.G. Biomimetic design and fabrication of porous chitosan–gelatin liver scaffolds with hierarchical channel network. *J. Mater. Sci. Mater. Med.* **2014**, *25*, 113–120. [CrossRef]
11. Onuma, Y.; Ormiston, J.; Serruys, P.W. Bioresorbable scaffold technologies. *Circ. J.* **2011**, *75*, 509. [CrossRef]
12. Bakhsheshi-Rad, H.R.; Hamzah, E.; Ismail, A.F.; Daroonparvar, M.; Yajid, M.A.M.; Medraj, M. Preparation and characterization of NiCrAlY/nano-YSZ/PCL composite coatings obtained by combination of atmospheric plasma spraying and dip coating on Mg–Ca alloy. *J. Alloys Compd.* **2016**, *658*, 440–452. [CrossRef]
13. Sanchez, A.H.M.; Luthringer, B.J.C.; Feyerabend, F.; Willumeit, R. Mg and Mg alloys: How comparable are in vitro and in vivo corrosion rates? A review. *Acta Biomater.* **2015**, *13*, 16–31. [CrossRef] [PubMed]
14. Staiger, M.P.; Pietak, A.M.; Huadmai, J.; Dias, G. Magnesium and its alloys as orthopedic biomaterials: A review. *Biomaterials* **2006**, *27*, 1728–1734. [CrossRef] [PubMed]
15. Witte, F.; Hort, N.; Vogt, C.; Cohen, S.; Kainer, K.U.; Willumeit, R.; Feyerabend, F. Degradable biomaterials based on magnesium corrosion. *Curr. Opin. Solid State Mater. Sci.* **2008**, *12*, 63–72. [CrossRef]
16. Chen, Y.; Xu, Z.; Smith, C.; Sankar, J. Recent advances on the development of magnesium alloys for biodegradable implants. *Acta Biomater.* **2014**, *10*, 4561–4573. [CrossRef]

17. Dayaghi, E.; Bakhsheshi-Rad, H.R.; Hamzah, E.; Akhavan-Farid, A.; Ismail, A.F.; Aziz, M.; Abdolahi, E. Magnesium-zinc scaffold loaded with tetracycline for tissue engineering application: In vitro cell biology and antibacterial activity assessment. *Mater. Sci. Eng. C* **2019**, *102*, 53–65. [CrossRef]
18. Xiong, P.; Jia, Z.; Li, M.; Zhou, W.; Yan, J.; Wu, Y.; Cheng, Y.; Zheng, Y. Biomimetic Ca, Sr/P-doped silk fibroin films on Mg-1Ca alloy with dramatic corrosion resistance and osteogenic activities. *ACS Biomater. Sci. Eng.* **2018**, *4*, 3163–3176. [CrossRef]
19. Nicolini, C.; Gupta, M. High Performance Lightweight Magnesium Nanocomposites for Engineering and Biomedical Applications. *Nano World J.* **2016**, *2*, 78–83.
20. Miracle, D.B.; Donaldson, S.L.; Henry, S.D.; Moosbrugger, C.; Anton, G.J.; Sanders, B.R.; Hrivnak, N.; Terman, C.; Kinson, J.; Muldoon, K.; et al. *ASM Handbook: Composite*; ASM International: Geauga, OH, USA, 2001; Volume 21.
21. Thakur, S.K.; Kwee, G.T.; Gupta, M. Development and characterization of magnesium composites containing nano-sized silicon carbide and carbon nanotubes as hybrid reinforcements. *J. Mater. Sci.* **2007**, *42*, 10040–10046. [CrossRef]
22. Razzaghi, M.; Kasiri-Asgarani, M.; Bakhsheshi-Rad, H.R.; Ghayour, H. Microstructure, mechanical properties, and in-vitro biocompatibility of nano-NiTi reinforced Mg–3Zn-0.5Ag alloy: Prepared by mechanical alloying for implant applications. *Compos. Part B Eng.* **2020**, *190*, 107947. [CrossRef]
23. Goh, C.S.; Wei, J.; Lee, L.C.; Gupta, M. Properties and deformation behaviour of Mg–Y_2O_3 nanocomposites. *Acta Mater.* **2007**, *55*, 5115–5121. [CrossRef]
24. Hassan, S.F.; Gupta, M. Development of high performance magnesium nano-composites using nano-Al_2O_3 as reinforcement. *Mater Sci. Eng. A* **2005**, *392*, 163–168. [CrossRef]
25. Sankaranarayanan, S.; Nayak, U.P.; Sabat, R.K.; Suwas, S.; Almajid, A.; Gupta, M. Nano-ZnO particle addition to monolithic magnesium for enhanced tensile and compressive response. *J. Alloys Compd.* **2014**, *615*, 211–219. [CrossRef]
26. Meenashisundaram, G.K.; Seetharaman, S.; Gupta, M. Enhancing overall tensile and compressive response of pure Mg using nano-TiB2 particulates. *Mater. Charact.* **2014**, *94*, 178–188. [CrossRef]
27. Tjong, S.C. Recent progress in the development and properties of novel metal matrix nanocomposites reinforced with carbon nanotubes and graphene nanosheets. *Mater. Sci. Eng. R Rep.* **2013**, *74*, 281–350. [CrossRef]
28. Tjong, S.C. Novel nanoparticle-reinforced metal matrix composites with enhanced mechanical properties. *Adv. Eng. Mater.* **2007**, *9*, 639–652. [CrossRef]
29. Haghshenas, M. Mechanical characteristics of biodegradable magnesium matrix composites: A review. *J. Magnes Alloy* **2017**, *5*, 189–201. [CrossRef]
30. Munir, K.; Wen, C.; Li, Y. Graphene nanoplatelets-reinforced magnesium metal matrix nanocomposites with superior mechanical and corrosion performance for biomedical applications. *J. Magnes Alloy* **2020**, *828*, 154461. [CrossRef]
31. Li, Y.; Feng, Z.; Huang, L.; Essa, K.; Bilotti, E.; Zhang, H.; Peijs, T.; Hao, L. Additive manufacturing high performance graphene-based composites: A review. *Compos. Part A Appl. Sci. Manuf.* **2019**, *124*, 105483. [CrossRef]
32. Gao, C.; Feng, P.; Peng, S.; Shuai, C. Carbon nanotube, graphene and boron nitride nanotube reinforced bioactive ceramics for bone repair. *Acta Biomater.* **2017**, *61*, 1–20. [CrossRef]
33. Shuai, C.; Liu, T.; Gao, C.; Feng, P.; Xiao, T.; Yu, K.; Peng, S. Mechanical and structural characterization of diopside scaffolds reinforced with graphene. *J. Alloys Compd.* **2016**, *655*, 86–92. [CrossRef]
34. Liu, C.; Shen, J.; Yeung, K.W.K.; Tjong, S.C. Development and antibacterial performance of novel polylactic acid-graphene oxide-silver nanoparticle hybrid nanocomposite mats prepared by electrospinning. *ACS Biomater. Sci. Eng.* **2017**, *3*, 471–486. [CrossRef]
35. Rashad, M.; Pan, F.; Yu, Z.; Asif, M.; Lin, H.; Pan, R. Investigation on microstructural, mechanical and electrochemical properties of aluminum composites reinforced with graphene nanoplatelets. *Prog. Nat. Sci. Mater. Int.* **2015**, *25*, 460–470. [CrossRef]
36. Saris, N.-E.L.; Mervaala, E.; Karppanen, H.; Khawaja, J.A.; Lewenstam, A. Magnesium: An update on physiological, clinical and analytical aspects. *Clin. Chim. Acta* **2000**, *294*, 1–26. [CrossRef]
37. Song, G.; Atrens, A. Understanding magnesium corrosion—a framework for improved alloy performance. *Adv. Eng. Mater.* **2003**, *5*, 837–858. [CrossRef]

38. Witte, F. The history of biodegradable magnesium implants: A review. *Acta Biomater.* **2010**, *6*, 1680–1692. [CrossRef]
39. Zhao, D.; Witte, F.; Lu, F.; Wang, J.; Li, J.; Qin, L. Current status on clinical applications of magnesium-based orthopaedic implants: A review from clinical translational perspective. *Biomaterials* **2017**, *112*, 287–302. [CrossRef]
40. Rodrigues, L.R. Inhibition of bacterial adhesion on medical devices. In *Bacterial Adhesion*; Springer: Dordrecht, The Netherlands, 2011; Volume 715, pp. 351–367.
41. Bellucci, D.; Cannillo, V.; Cattini, A.; Sola, A. A new generation of scaffolds for bone tissue engineering. *Ind. Ceram.* **2011**, *31*, 59–62. [CrossRef]
42. Boccaccini, A.R.; Blaker, J.J. Bioactive composite materials for tissue engineering scaffolds. *Expert Rev. Med. Devices* **2005**, *2*, 303–317. [CrossRef]
43. Mouriño, V.; Boccaccini, A.R. Bone tissue engineering therapeutics: Controlled drug delivery in three-dimensional scaffolds. *J. R Soc. Interface* **2010**, *7*, 209–227. [CrossRef]
44. Hornberger, H.; Virtanen, S.; Boccaccini, A.R. Biomedical coatings on magnesium alloys—A review. *Acta Biomater.* **2012**, *8*, 2442–2455. [CrossRef] [PubMed]
45. Ali, M.; Hussein, M.A.; Al-Aqeeli, N. Magnesium-based composites and alloys for medical applications: A review of mechanical and corrosion properties. *J. Alloys Compd.* **2019**, *792*, 1162–1190. [CrossRef]
46. Prakasam, M.; Locs, J.; Salma-Ancane, K.; Loca, D.; Largeteau, A.; Berzina-Cimdina, L. Biodegradable materials and metallic implants—a review. *J. Funct. Biomater.* **2017**, *8*, 44. [CrossRef] [PubMed]
47. Munir, K.S.; Wen, C.; Li, Y. Carbon nanotubes and graphene as nanoreinforcements in metallic biomaterials: A review. *Adv. Biosyst.* **2019**, *3*, 1800212. [CrossRef] [PubMed]
48. Yunus Basha, R.T.S.S.K.; Doble, M. Design of biocomposite materials for bone tissue regeneration. *Mater Sci. Eng., C* **2015**, *57*, 452–463. [CrossRef] [PubMed]
49. Xie, H.; Cao, T.; Rodríguez-Lozano, F.J.; Luong-Van, E.K.; Rosa, V. Graphene for the development of the next-generation of biocomposites for dental and medical applications. *Dent. Mater.* **2017**, *33*, 765–774. [CrossRef] [PubMed]
50. Hu, W.; Peng, C.; Luo, W.; Lv, M.; Li, X.; Li, D.; Huang, Q.; Fan, C. Graphene-Based Antibacterial Paper. *ACS Nano.* **2010**, *4*, 4317. [CrossRef]
51. Bakhsheshi-Rad, H.R.; Hamzah, E.; Kasiri-Asgarani, M.; Saud, S.N.; Yaghoubidoust, F.; Akbari, E. Structure, corrosion behavior, and antibacterial properties of nano-silica/graphene oxide coating on biodegradable magnesium alloy for biomedical applications. *Vacuum* **2016**, *131*, 106–110. [CrossRef]
52. Krishnamoorthy, K.; Veerapandian, M.; Zhang, L.-H.; Yun, K.; Kim, S.J. Antibacterial efficiency of graphene nanosheets against pathogenic bacteria via lipid peroxidation. *J. Phys. Chem. C* **2012**, *116*, 17280–17287. [CrossRef]
53. Loh, K.P.; Bao, Q.; Ang, P.K.; Yang, J. The chemistry of graphene. *J. Mater. Chem.* **2010**, *20*, 2277–2289. [CrossRef]
54. Gurunathan, S.; Han, J.W.; Dayem, A.A.; Eppakayala, V.; Park, M.R.; Kwon, D.N.; Kim, J.H. Antibacterial activity of dithiothreitol reduced graphene oxide. *J. Ind. Eng. Chem.* **2013**, *19*, 1280–1288. [CrossRef]
55. Akhavan, O.; Ghaderi, E. Toxicity of graphene and graphene oxide nanowalls against bacteria. *ACS Nano.* **2010**, *4*, 5731–5736. [CrossRef] [PubMed]
56. Chen, J.; Peng, H.; Wang, X.; Shao, F.; Yuan, Z.; Han, H. Graphene oxide exhibits broad-spectrum antimicrobial activity against bacterial phytopathogens and fungal conidia by intertwining and membrane perturbation. *Nanoscale* **2014**, *6*, 1879–1889. [CrossRef] [PubMed]
57. Liu, S.; Zeng, T.H.; Hofmann, M.; Burcombe, E.; Wei, J.; Jiang, R.; Kong, J.; Chen, Y. Antibacterial activity of graphite, graphite oxide, graphene oxide, and reduced graphene oxide: Membrane and oxidative stress. *ACS Nano.* **2011**, *5*, 6971–6980. [CrossRef] [PubMed]
58. Chen, J.; Wang, X.; Han, H. A new function of graphene oxide emerges: Inactivating phytopathogenic bacterium Xanthomonas oryzae pv. Oryzae. *J. Nanopart. Res.* **2013**, *15*, 1658. [CrossRef]
59. Ahmed, F.; Rodrigues, D.F. Investigation of acute effects of graphene oxide on wastewater microbial community: A case study. *J. Hazard Mater.* **2013**, *256*, 33–39. [CrossRef] [PubMed]
60. Gurunathan, S.; Han, J.W.; Dayem, A.A.; Eppakayala, V.; Kim, J.-H. Oxidative stress-mediated antibacterial activity of graphene oxide and reduced graphene oxide in Pseudomonas aeruginosa. *Int. J. Nanomed.* **2012**, *7*, 5901. [CrossRef]

61. Park, S.; Ruoff, R.S. Chemical methods for the production of graphenes. *Nat. Nanotechnol.* **2009**, *4*, 217–224. [CrossRef]
62. Novoselov, K.S.; Geim, A.K.; Morozov, S.V.; Jiang, D.; Zhang, Y.; Dubonos, S.V. Electric field effect in atomically thin carbon films. *Science* **2004**, *306*, 666–669. [CrossRef]
63. Eizenberg, M.; Blakely, J.M. Carbon monolayer phase condensation on Ni (111). *Surf. Sci.* **1979**, *82*, 228–236. [CrossRef]
64. Aizawa, T.; Souda, R.; Otani, S.; Ishizawa, Y.; Oshima, C. Anomalous bond of monolayer graphite on transition-metal carbide surfaces. *Phys. Rev. Lett.* **1990**, *64*, 768. [CrossRef] [PubMed]
65. Berger, C.; Song, Z.; Li, X.; Wu, X.; Brown, N.; Naud, C.; Mayou, D.; Li, T.; Hass, J. Electronic confinement and coherence in patterned epitaxial graphene. *Science* **2006**, *312*, 1191–1196. [CrossRef] [PubMed]
66. Stankovich, S.; Piner, R.D.; Nguyen, S.T.; Ruoff, R.S. Synthesis and exfoliation of isocyanate-treated graphene oxide nanoplatelets. *Carbon* **2006**, *44*, 3342–3347. [CrossRef]
67. Stankovich, S.; Piner, R.D.; Chen, X.; Wu, N.; Nguyen, S.T.; Ruoff, R.S. Stable aqueous dispersions of graphitic nanoplatelets via the reduction of exfoliated graphite oxide in the presence of poly (sodium 4-styrenesulfonate). *J. Mater. Chem.* **2006**, *16*, 155–158. [CrossRef]
68. Staudenmaier, L. Verfahren zur darstellung der graphitsäure. *Berichte der Dtsch. Chem. Gesellschaft.* **1898**, *31*, 1481–1487. [CrossRef]
69. Hummers, W.S.; Offeman, R.E. Preparation of Graphitic Oxide. *J. Am. Chem. Soc.* **1958**, *80*, 1339. [CrossRef]
70. Boehm, H.-P.; Clauss, A.; Fischer, G.O.; Hofmann, U. Das adsorptionsverhalten sehr dünner kohlenstoff-folien. *Zeitschrift für Anorg. und Allg. Chemie* **1962**, *316*, 119–127. [CrossRef]
71. Stankovich, S.; Dikin, D.A.; Dommett, G.H.; Kohlhaas, K.M.; Zimney, E.J.; Stach, E.A.; Piner, R.D.; Nguyen, S.T.; Ruoff, R.S. Graphene-based composite Materials. *Nature* **2006**, *442*, 282–286.
72. Schniepp, H.C.; Li, J.L.; McAllister, M.J.; Sai, H.; Herrera-Alonso, M.; Adamson, D.H.; Prud'homme, R.K.; Car, R.; Saville, D.A.; Aksay, I.A. Functionalized single graphene sheets derived from splitting graphite oxide. *J. Phys. Chem. B* **2006**, *110*, 8535–8539. [CrossRef]
73. McAllister, M.J.; Li, J.; Adamson, D.H.; Schniepp, H.C.; Abdala, A.A.; Liu, J.; Herrera-Alonso, M.; Milius, D.L.; Car, R.; Prud'homme, R.K.; et al. Single sheet functionalized graphene by oxidation and thermal expansion of graphite. *Chem. Mater.* **2007**, *19*, 4396–4404. [CrossRef]
74. Kumar, H.G.P.; Xavior, M.A. Graphene reinforced metal matrix composite (GRMMC): A review. *Procedia Eng.* **2014**, *97*, 1033–1040. [CrossRef]
75. Rodriguez, C.L.C.; Kessler, F.; Dubey, N.; Rosa, V.; Fechine, G.J.M. CVD graphene transfer procedure to the surface of stainless steel for stem cell proliferation. *Surf. Coat. Technol.* **2017**, *311*, 10–18. [CrossRef]
76. Pei, S.; Cheng, H.-M. The reduction of graphene oxide. *Carbon* **2012**, *50*, 3210–3228. [CrossRef]
77. Dreyer, D.R.; Park, S.; Bielawski, C.W. RS Ruoff The chemistry of graphene oxide. *Chem. Soc. Rev.* **2010**, *39*, 228–240. [CrossRef] [PubMed]
78. Rosa, V.; Xie, H.; Dubey, N.; Madanagopal, T.T.; Rajan, S.S.; Morin, J.L.P.; Islam, I.; Neto, A.H.C. Graphene oxide-based substrate: Physical and surface characterization, cytocompatibility and differentiation potential of dental pulp stem cells. *Dent Mater.* **2016**, *32*, 1019–1025. [CrossRef]
79. Choi, W.; Lahiri, I.; Seelaboyina, R.; Kang, Y.S. Synthesis of graphene and its applications: A review. *Crit. Rev. Solid State Mater. Sci.* **2010**, *35*, 52–71. [CrossRef]
80. Zhu, Y.; Murali, S.; Cai, W.; Li, X.; Suk, J.W.; Potts, J.R.; Ruoff, R.S. Graphene and graphene oxide: Synthesis, properties, and applications. *Adv. Mater.* **2010**, *22*, 3906–3924. [CrossRef]
81. Lee, C.; Wei, X.; Kysar, J.W.; Hone, J. Measurement of the elastic properties and intrinsic strength of monolayer graphene. *Science* **2008**, *321*, 385–388. [CrossRef]
82. Jeon, C.H.; Jeong, Y.H.; Seo, J.J.; Tien, H.N.; Hong, S.T.; Yum, Y.J.; Hur, S.H.; Lee, K.J. Material properties of graphene/aluminum metal matrix composites fabricated by friction stir processing. *Int. J. Precis Eng. Manuf.* **2014**, *15*, 1235–1239. [CrossRef]
83. Xiang, S.; Wang, X.; Gupta, M.; Wu, K.; Hu, X.; Zheng, M. Graphene nanoplatelets induced heterogeneous bimodal structural magnesium matrix composites with enhanced mechanical properties. *Sci. Rep.* **2016**, *6*, 38824. [CrossRef]
84. Tabandeh-Khorshid, M.; Kumar, A.; Omrani, E.; Kim, C.; Rohatgi, P. Synthesis, characterization, and properties of graphene reinforced metal-matrix nanocomposites. *Compos. Part B Eng.* **2020**, *183*, 107664. [CrossRef]

85. Salleh, E.M.; Zuhailawati, H.; Ramakrishnan, S.; Dhindaw, B.K. Enhanced mechanical properties and corrosion behavior of biodegradable Mg-Zn/HA composite. *Metall. Mater. Trans. A* **2017**, *48*, 2519–2528. [CrossRef]
86. Khalajabadi, S.Z.; Kadir, M.R.A.; Izman, S.; Bakhsheshi-Rad, H.R.; Farahany, S. Effect of mechanical alloying on the phase evolution, microstructure and bio-corrosion properties of a Mg/HA/TiO_2/MgO nanocomposite. *Ceram. Int.* **2014**, *40*, 16743–16759. [CrossRef]
87. Saheban, M.; Bakhsheshi-Rad, H.R.; Hamzah, E.; Ismail, A.F.; Aziz, M.; Hamzah, E.; Najafinezhad, A. Effect of zeolite on the corrosion behavior, biocompatibility and antibacterial activity of porous magnesium/zeolite composite scaffolds. *Mater. Technol.* **2019**, *34*, 258–269. [CrossRef]
88. Wan, Y.; Cui, T.; Li, W.; Li, C.; Xiao, J.; Zhu, Y.; Ji, D.; Xiong, G.; Luo, H. Mechanical and biological properties of bioglass/magnesium composites prepared via microwave sintering route. *J. Compos. Mater.* **2016**, *99*, 521–527. [CrossRef]
89. Zheng, Y.F.; Gu, X.N.; Xi, Y.L.; Chai, D.L. In vitro degradation and cytotoxicity of Mg/Ca composites produced by powder metallurgy. *Acta Biomater.* **2010**, *6*, 1783–1791. [CrossRef]
90. Chen, L.Y.; Konishi, H.; Fehrenbacher, A.; Ma, C.; Xu, J.Q.; Choi, H.; Xu, H.F.; Pfefferkorn, F.E.; Li, X.C. Novel nanoprocessing route for bulk graphene nanoplatelets reinforced metal matrix nanocomposites. *Scr. Mater.* **2012**, *67*, 29–32. [CrossRef]
91. Rashad, M.; Pan, F.; Tang, A.; Asif, M.; She, J.; Gou, J.; Mao, J.; Hu, H. Development of magnesium-graphene nanoplatelets composite. *J Compos. Mater.* **2015**, *49*, 285–293. [CrossRef]
92. Du, X.; Du, W.; Wang, Z.; Liu, K.; Li, S. Ultra-high strengthening efficiency of graphene nanoplatelets reinforced magnesium matrix composites. *Mater. Sci. Eng. A* **2018**, *711*, 633–642. [CrossRef]
93. Yang, Z.; Xu, H.; Wang, Y.; Hu, M.; Ji, Z. Investigation of the microstructure and mechanical properties of AZ31/graphene composite fabricated by semi-solid isothermal treatment and hot extrusion. *JOM* **2019**, *71*, 4162–4170. [CrossRef]
94. Shahin, M.; Munir, K.; Wen, C.; Li, Y. Magnesium-based composites reinforced with graphene nanoplatelets as biodegradable implant materials. *J. Alloys Compd.* **2020**, *828*, 154461. [CrossRef]
95. Rashad, M.; Pan, F.; Lin, D.; Asif, M. High temperature mechanical behavior of AZ61 magnesium alloy reinforced with graphene nanoplatelets. *J. Compos. Mater.* **2016**, *89*, 1242–1250. [CrossRef]
96. Ramezanzade, S.; Ebrahimi, G.R.; Parizi, M.T.; Ezatpour, H.R. Microstructure and mechanical characterizations of graphene nanoplatelets-reinforced Mg–Sr–Ca alloy as a novel composite in structural and biomedical applications. *J. Compos. Mater.* **2020**, *54*, 711–728. [CrossRef]
97. Wang, M.; Zhao, Y.; Wang, L.D.; Zhu, Y.P.; Wang, X.J.; Sheng, J.; Yang, Z.Y.; Shi, H.L.; Shi, Z.D.; Fei, W.D. Achieving high strength and ductility in graphene/magnesium composite via an in-situ reaction wetting process. *Carbon* **2018**, *139*, 954–963. [CrossRef]
98. Du, X.; Du, W.; Wang, Z.; Liu, K.; Li, S. Defects in graphene nanoplatelets and their interface behavior to reinforce magnesium alloys. *Appl. Surf. Sci.* **2019**, *484*, 414–423. [CrossRef]
99. Xiang, S.L.; Gupta, M.; Wang, X.J.; Wang, L.D.; Hu, X.S.; Wu, K. Enhanced overall strength and ductility of magnesium matrix composites by low content of graphene nanoplatelets. *Compos. Part A Appl. Sci. Manuf.* **2017**, *100*, 183–193. [CrossRef]
100. Rashad, M.; Pan, F.; Asif, M. Exploring mechanical behavior of Mg–6Zn alloy reinforced with graphene nanoplatelets. *Mater. Sci. Eng. A* **2016**, *649*, 263–269. [CrossRef]
101. Arab, M.; Marashi, S.P.H. Graphene nanoplatelet (GNP)-incorporated AZ31 magnesium nanocomposite: Microstructural, mechanical and tribological properties. *Tribol. Lett.* **2018**, *66*, 156. [CrossRef]
102. Shuai, C.; Wang, B.; Yang, Y.; Peng, S.; Gao, C. 3D honeycomb nanostructure-encapsulated magnesium alloys with superior corrosion resistance and mechanical properties. *Compos. Part B Eng.* **2019**, *162*, 611–620. [CrossRef]
103. Chen, L.-Y.; Peng, J.-Y.; Xu, J.-Q.; Choi, H.; Li, X.-C. Achieving uniform distribution and dispersion of a high percentage of nanoparticles in metal matrix nanocomposites by solidification processing. *Scr. Mater.* **2013**, *69*, 634–637. [CrossRef]
104. Nie, K.B.; Wang, X.J.; Wu, K.; Xu, L.; Zheng, M.Y.; Hu, X.S. Processing, microstructure and mechanical properties of magnesium matrix nanocomposites fabricated by semisolid stirring assisted ultrasonic vibration. *J. Alloys Compd.* **2011**, *509*, 8664–8669. [CrossRef]

105. Turan, M.E.; Sun, Y.; Akgul, Y. Mechanical, tribological and corrosion properties of fullerene reinforced magnesium matrix composites fabricated by semi powder metallurgy. *J. Alloys Compd.* **2018**, *740*, 1149–1158. [CrossRef]
106. Turan, M.E.; Zengin, H.; Sun, Y. Dry sliding wear behavior of (MWCNT + GNPs) reinforced AZ91 magnesium matrix hybrid composites. *Met. Mater. Int.* **2020**, *26*, 540–550. [CrossRef]
107. Turan, M.E.; Sun, Y.; Akgul, Y.; Turen, Y.; Ahlatci, H. The effect of GNPs on wear and corrosion behaviors of pure magnesium. *J. Alloys Compd.* **2017**, *724*, 14–23. [CrossRef]
108. Turan, M.E.; Sun, Y.; Aydin, F.; Zengin, H.; Turen, Y.; Ahlatci, H. Effects of carbonaceous reinforcements on microstructure and corrosion properties of magnesium matrix composites. *Mater. Chem. Phys.* **2018**, *218*, 182–188. [CrossRef]
109. Rashad, M.; Pan, F.; Asif, M.; Tang, A. Powder metallurgy of Mg–1%Al–1%Sn alloy reinforced with low content of graphene nanoplatelets (GNPs). *J. Ind. Eng. Chem.* **2014**, *20*, 4250–4255. [CrossRef]
110. Saberi, A.; Bakhsheshi-Rad, H.R.; Karamian, E.; Kasiri-Asgarani, M.; Ghomi, H. Magnesium-graphene nano-platelet composites: Corrosion behavior, mechanical and biological properties. *J. Alloys Compd.* **2020**, *821*, 153379. [CrossRef]
111. Rashad, M.; Pan, F.; Tang, A.; Asif, M.; Aamir, M. Synergetic effect of graphene nanoplatelets (GNPs) and multi-walled carbon nanotube (MW-CNTs) on mechanical properties of pure magnesium. *J. Alloys Compd.* **2014**, *603*, 111–118. [CrossRef]
112. Rafiee, M.A.; Rafiee, J.; Srivastava, I.; Wang, Z.; Song, H.; Yu, Z.Z.; Koratkar, N. Fracture and fatigue in graphene nanocomposites. *Small* **2010**, *6*, 179–183. [CrossRef]
113. Ferguson, J.B.; Schultz, B.F.; Venugopalan, D.; Lopez, H.F.; Rohatgi, P.K.; Cho, K.; Kim, C.-S. On the superposition of strengthening mechanisms in dispersion strengthened alloys and metal-matrix nanocomposites: Considerations of stress and energy. *Met. Mater. Int.* **2014**, *20*, 375–388. [CrossRef]
114. Ramezanzade, S.; Ebrahimi, G.R.; Parizi, M.T.; Ezatpour, H.R. Synergetic effect of GNPs and MgOs on the mechanical properties of Mg–Sr–Ca alloy. *Mater. Sci. Eng. A* **2019**, *761*, 138025. [CrossRef]
115. Meng, L.; Hu, X.; Wang, X.; Zhang, C.; Shi, H.; Xiang, Y.; Liu, N.; Wu, K. Graphene nanoplatelets reinforced Mg matrix composite with enhanced mechanical properties by structure construction. *Mater. Sci. Eng. A* **2018**, *733*, 414–418. [CrossRef]
116. Yuan, Q.; Zhou, G.; Liao, L.; Liu, Y.; Luo, L. Interfacial structure in AZ91 alloy composites reinforced by graphene nanosheets. *Carbon* **2018**, *127*, 177–186. [CrossRef]
117. Kandemir, S. Development of Graphene Nanoplatelet-Reinforced AZ91 Magnesium Alloy by Solidification Processing. *J Mater. Eng. Perform.* **2018**, *27*, 3014–3023. [CrossRef]
118. Rashad, M.; Pan, F.; Tang, A.; Asif, M.; Hussain, S.; Gou, J.; Mao, J. Improved strength and ductility of magnesium with addition of aluminum and graphene nanoplatelets (Al + GNPs) using semi powder metallurgy method. *J. Ind. Eng. Chem.* **2015**, *23*, 243–250. [CrossRef]
119. Rashad, M.; Pan, F.S.; Asif, M.; Ullah, A. Improved mechanical properties of magnesium–graphene composites with copper–graphene hybrids. *Mater. Sci. Technol.* **2015**, *31*, 1452–1461. [CrossRef]
120. Rashad, M.; Pan, F.; Asif, M. Magnesium matrix composites reinforced with graphene nanoplatelets. *Graphene Mater. Sci. Eng. A* **2015**, *630*, 36–44. [CrossRef]
121. Clyne, T.W.; Withers, P.J. *An Introduction to Metal Matrix Composites*; Cambridge university press: Cambridge, UK, 1995.
122. Courtney, T.H. *Mechanical Behavior of Materials*; Waveland Press: Long Grove, IL, USA, 2005.
123. Şenel, M.C.; Gürbüz, M.; Koc, E. Fabrication and characterization of synergistic Al-SiC-GNPs hybrid composites. *Compos. Part B Eng.* **2018**, *154*, 1–9. [CrossRef]
124. Tiwari, A.; Syväjärvi, M. *Graphene Materials: Fundamentals and Emerging Applications*; John Wiley & Sons: Hoboken, NJ, USA, 2015.
125. Rashad, M.; Pan, F.; Zhang, J.; Asif, M. Use of high energy ball milling to study the role of graphene nanoplatelets and carbon nanotubes reinforced magnesium alloy. *J. Alloys Compd.* **2015**, *646*, 223–232. [CrossRef]
126. Rashad, M.; Pan, F.; Liu, Y.; Chen, X.; Lin, H.; Pan, R.; Asif, M.; She, J. High temperature formability of graphene nanoplatelets-AZ31 composites fabricated by stir-casting method. *J. Magnes Alloy* **2016**, *4*, 270–277. [CrossRef]

127. Torabi Parizi, M.; Ebrahimi, G.R.; Ezatpour, H.R. Effect of graphene nanoplatelets content on the microstructural and mechanical properties of AZ80 magnesium alloy. *Mater. Sci. Eng. A* **2019**, *742*, 373–389. [CrossRef]
128. Rashad, M.; Pan, F.; Tang, A.; Lu, Y.; Asif, M.; Hussain, S.; She, J.; Gou, J.; Mao, J. Effect of graphene nanoplatelets (GNPs) addition on strength and ductility of magnesium-titanium alloys. *J. Magnes Alloy* **2013**, *1*, 242–248. [CrossRef]
129. Manivasagam, G.; Suwas, S. Biodegradable Mg and Mg based alloys for biomedical implants. *Mater. Sci. Technol.* **2014**, *30*, 515–520. [CrossRef]
130. Gu, X.N.; Zheng, W.; Cheng, Y.; Zheng, Y.F. A study on alkaline heat treated Mg–Ca alloy for the control of the biocorrosion rate. *Acta Biomater.* **2009**, *5*, 2790–2799. [CrossRef] [PubMed]
131. Lloyd, A.W. Interfacial bioengineering to enhance surface biocompatibility. *Med. Device Technol.* **2002**, *13*, 18–21.
132. Ruedi, T.P. *AO principles of fracture management*; Thieme: New York, NY, USA, 2000.
133. Erinc, M.; Sillekens, W.H.; Mannens, R.; Werkhoven, R.J. Applicability of existing magnesium alloys as biomedical implant Materials. In Proceedings of the Magnesium Technology 2009, San Francisco, CA, USA, 15–19 February 2009; pp. 209–214, Conference code: 76923.
134. Atrens, A.D.; Gentle, I.; Atrens, A. Possible dissolution pathways participating in the Mg corrosion reaction. *Corros. Sci.* **2015**, *92*, 173–181. [CrossRef]
135. Xin, Y.; Huo, K.; Tao, H.; Tang, G.; Chu, P.K. Influence of aggressive ions on the degradation behavior of biomedical magnesium alloy in physiological environment. *Acta Biomater.* **2008**, *4*, 2008–2015. [CrossRef]
136. Raucci, M.G.; Giugliano, D.; Longo, A.; Zeppetelli, S.; Carotenuto, G.; Ambrosio, L. Comparative facile methods for preparing graphene oxide–hydroxyapatite for bone tissue engineering. *J. Tissue Eng. Regen Med.* **2017**, *11*, 2204–2216. [CrossRef]
137. Kurapati, R.; Russier, J.; Squillaci, M.A.; Treossi, E.; Ménard-Moyon, C.; Del Rio-Castillo, A.E.; Vazquez, E.; Samorì, P.; Palermo, V.; Bianco, A. Dispersibility-dependent biodegradation of graphene oxide by myeloperoxidase. *Small* **2015**, *11*, 3985–3994. [CrossRef]
138. Kirkland, N.T.; Schiller, T.; Medhekar, N.; Birbilis, N. Exploring graphene as a corrosion protection barrier. *Corros. Sci.* **2012**, *56*, 1–4. [CrossRef]
139. Raman, R.S.; Banerjee, P.C.; Lobo, D.E.; Gullapalli, H.; Sumandasa, M.; Kumar, A.; Choudhary, L.; Tkacz, R.; Ajayan, P.M.; Majumder, M. Protecting copper from electrochemical degradation by graphene coating. *Carbon* **2012**, *50*, 4040–4045. [CrossRef]
140. Neupane, M.P.; Lee, S.J.; Kang, J.Y.; Park, I.S.; Bae, T.S.; Lee, M.H. Surface characterization and corrosion behavior of silanized magnesium coated with graphene for biomedical application. *Mater. Chem. Phys.* **2015**, *163*, 229–235. [CrossRef]
141. Rashad, M.; Pan, F.; Asif, M.; Chen, X. Corrosion behavior of magnesium-graphene composites in sodium chloride solutions. *J. Magnes Alloy* **2017**, *5*, 271–276. [CrossRef]
142. Kavimani, V.; Soorya Prakash, K.; Arun Pandian, M. Influence of r-GO addition on enhancement of corrosion and wear behavior of AZ31 MMC. *Appl. Phys. A* **2017**, *123*, 514. [CrossRef]
143. Kavimani, V.; Soorya Prakash, K.; Thankachan, T. Investigation of graphene-reinforced magnesium metal matrix composites processed through a solvent-based powder metallurgy route. *Bull. Mater. Sci.* **2019**, *42*, 39. [CrossRef]
144. Aydin, F.; Ayday, A.; Turan, M.E.; Zengin, H. Role of graphene additive on wear and electrochemical corrosion behaviour of plasma electrolytic oxidation (PEO) coatings on Mg–MWCNT nanocomposite. *Surf. Eng.* **2019**, 1–9. [CrossRef]
145. Tsetseris, L.; Pantelides, S.T. Graphene: An impermeable or selectively permeable membrane for atomic species? *Carbon* **2014**, *67*, 58–63. [CrossRef]
146. Kotchey, G.P.; Allen, B.L.; Vedala, H.; Yanamala, N.; Kapralov, A.A.; Tyurina, Y.Y.; Klein-Seetharaman, J.; Kagan, V.E.; Star, A. The Enzymatic Oxidation of Graphene Oxide. *ACS Nano.* **2011**, *5*, 2098–2108. [CrossRef]
147. Bonaccorso, F.; Colombo, L.; Yu, G.; Stoller, M.; Tozzini, V.; Ferrari, A.C.; Ruoff, R.S.; Pellegrini, V. Graphene, related two-dimensional crystals, and hybrid systems for energy conversion and storage. *Science* **2015**, *347*, 1246501. [CrossRef]

148. Newman, L.; Lozano, N.; Zhang, M.; Iijima, S.; Yudasaka, M.; Bussy, C.; Kostarelos, K. Hypochlorite degrades 2D graphene oxide sheets faster than 1D oxidised carbon nanotubes and nanohorns. *NPJ 2D Mater. Appl.* **2017**, *1*, 1–9. [CrossRef]
149. Bal, B.S.; Rahaman, M.N. Orthopedic applications of silicon nitride ceramics. *Acta Biomater.* **2012**, *8*, 2889–2898. [CrossRef] [PubMed]
150. Shahin, M.; Munir, K.; Wen, C.; Li, Y. Magnesium matrix nanocomposites for orthopedic applications: A review from mechanical, corrosion, and biological perspectives. *Acta Biomater.* **2019**, *96*, 1–19. [CrossRef] [PubMed]
151. Shen, J.; Shi, M.; Yan, B.; Ma, H.; Li, N.; Hu, Y.; Ye, M. Covalent attaching protein to graphene oxide via diimide-activated amidation. *Colloids Surf., B* **2010**, *81*, 434–438. [CrossRef] [PubMed]
152. Girase, B.; Shah, J.S.; Misra, R.D.K. Cellular mechanics of modulated osteoblasts functions in graphene oxide reinforced elastomers. *Adv. Eng. Mater.* **2012**, *14*, 101–111. [CrossRef]
153. Neagu, M.; Piperigkou, Z.; Karamanou, K.; Engin, A.B.; Docea, A.O.; Constantin, C.; Negrei, C.; Nikitovic, D.; Tsatsakis, A. Protein bio-corona: Critical issue in immune nanotoxicology. *Arch. Toxicol.* **2017**, *91*, 1031–1048. [CrossRef]
154. La, W.G.; Jin, M.; Park, S.; Yoon, H.H.; Jeong, G.J.; Bhang, S.H.; Park, H.; Char, K.; Kim, B.S. Delivery of bone morphogenetic protein-2 and substance P using graphene oxide for bone regeneration. *Int. J. Nanomed.* **2014**, *9*, 107–116.
155. Ku, S.H.; Park, C.B. Myoblast differentiation on graphene oxide. *Biomaterials* **2013**, *34*, 2017–2023. [CrossRef]
156. Hronik-Tupaj, M.; Rice, W.L.; Cronin-Golomb, M.; Kaplan, D.L.; Georgakoudi, I. Osteoblastic differentiation and stress response of human mesenchymal stem cells exposed to alternating current electric fields. *Biomed. Eng. Online* **2011**, *10*, 9. [CrossRef]
157. Aaron, R.K.; Boyan, B.D.; Ciombor, D.M.; Schwartz, Z.; Simon, B.J. Stimulation of growth factor synthesis by electric and electromagnetic fields. *Clin. Orthop. Relat. Res.* **2004**, *419*, 30–37. [CrossRef]
158. Gong, H.; Anasori, B.; Dennison, C.R.; Wang, K.; Kumbur, E.C.; Strich, R.; Zhou, J.G. Fabrication, biodegradation behavior and cytotoxicity of Mg-nanodiamond composites for implant application. *J. Mater. Sci. Mater. Med.* **2015**, *26*, 110. [CrossRef]
159. Nanda, S.S.; Yi, D.K.; Kim, K. Study of antibacterial mechanism of graphene oxide using Raman spectroscopy. *Sci. Rep.* **2016**, *6*, 1–12. [CrossRef]
160. Hegab, H.M.; ElMekawy, A.; Zou, L.; Mulcahy, D.; Saint, C.P.; Ginic-Markovic, M. The controversial antibacterial activity of graphene-based Materials. *Carbon* **2016**, *105*, 362–376. [CrossRef]
161. Li, C.; Wang, X.; Chen, F.; Zhang, C.; Zhi, X.; Wang, K.; Cui, D. The antifungal activity of graphene oxide–silver nanocomposites. *Biomaterials* **2013**, *34*, 3882–3890. [CrossRef] [PubMed]
162. Zhao, R.; Kong, W.; Sun, M.; Yang, Y.; Liu, W.; Lv, M.; Song, S.; Wang, L.; Song, H.; Hao, R. Highly stable graphene-based nanocomposite (GO–PEI–Ag) with broad-spectrum, long-term antimicrobial activity and antibiofilm effects. *ACS Appl. Mater. Interfaces* **2018**, *10*, 17617–17629. [CrossRef] [PubMed]
163. Zou, X.; Zhang, L.; Wang, Z.; Luo, Y. Mechanisms of the antimicrobial activities of graphene Materials. *J. Am. Chem. Soc.* **2016**, *138*, 2064–2077. [CrossRef] [PubMed]
164. Shuai, C.; Guo, W.; Wu, P.; Yang, W.; Hu, S.; Xia, Y.; Feng, P. A graphene oxide-Ag co-dispersing nanosystem: Dual synergistic effects on antibacterial activities and mechanical properties of polymer scaffolds. *Chem. Eng. J.* **2018**, *347*, 322–333. [CrossRef]
165. Saito, N.; Haniu, H.; Usui, Y.; Aoki, K.; Hara, K.; Takanashi, S.; Shimizu, M.; Narita, N.; Okamoto, M.; Kobayashi, S.; et al. Safe clinical use of carbon nanotubes as innovative Biomaterials. *Chem. Rev.* **2014**, *114*, 6040–6079. [CrossRef]
166. Rahim, M.I.; Ullah, S.; Mueller, P.P. Advances and challenges of biodegradable implant materials with a focus on magnesium-alloys and bacterial infections. *Metals* **2018**, *8*, 532. [CrossRef]
167. Peron, M.; Torgersen, J.; Berto, F. Mg and its alloys for biomedical applications: Exploring corrosion and its interplay with mechanical failure. *Metals* **2017**, *7*, 252. [CrossRef]
168. Azarniya, A.; Safavi, M.S.; Sovizi, S.; Azarniya, A.; Chen, B.; Madaah Hosseini, H.R.; Ramakrishna, S. Metallurgical challenges in carbon nanotube-reinforced metal matrix nanocomposites. *Metals* **2017**, *7*, 384. [CrossRef]
169. Liu, L.; Wang, J.; Russell, T.; Sankar, J.; Yun, Y. The biological responses to magnesium-based biodegradable medical devices. *Metals* **2017**, *7*, 514. [CrossRef]

170. Zhou, M.; Qu, X.; Ren, L.; Fan, L.; Zhang, Y.; Guo, Y.; Quan, G.; Tang, Q.; Liu, B.; Sun, H. The effects of carbon nanotubes on the mechanical and wear properties of AZ31 alloy. *Materials* **2017**, *10*, 1385. [CrossRef] [PubMed]
171. Saboori, A.; Dadkhah, M.; Fino, P.; Pavese, M. An overview of metal matrix nanocomposites reinforced with graphene nanoplatelets; mechanical, electrical and thermophysical properties. *Metals* **2018**, *8*, 423. [CrossRef]
172. Saboori, A.; Moheimani, S.K.; Dadkhah, M.; Pavese, M.; Badini, C.; Fino, P. An overview of key challenges in the fabrication of metal matrix nanocomposites reinforced by graphene nanoplatelets. *Metals* **2018**, *8*, 172. [CrossRef]
173. Kim, G.-N.; Kim, J.-H.; Kim, B.-S.; Jeong, H.-M.; Huh, S.-C. Study on the thermal conductivity characteristics of graphene prepared by the planetary ball mill. *Metals* **2016**, *6*, 234. [CrossRef]
174. Li, H.; Fan, L.; Zhou, M.; Zhou, Y.; Jiang, K.; Chen, Y. Hot compression deformation and activation energy of nanohybrid-reinforced AZ80 magnesium matrix composite. *Metals* **2020**, *10*, 119. [CrossRef]
175. Dai, Y.; Liu, H.; Tang, Y.; Xu, X.; Long, H.; Yan, Y.; Luo, Z.; Zhang, Y.; Yu, K.; Zhu, Y. A potential biodegradable Mg-Y-Ag implant with strengthened antimicrobial properties in orthopedic applications. *Metals* **2018**, *8*, 948. [CrossRef]
176. Kafri, A.; Ovadia, S.; Goldman, J.; Drelich, J.; Aghion, E. The suitability of Zn–1.3% Fe alloy as a biodegradable implant material. *Metals* **2018**, *8*, 153. [CrossRef]
177. Cao, N.Q.; Pham, D.N.; Kai, N.; Dinh, H.V.; Hiromoto, S.; Kobayashi, E. In vitro corrosion properties of Mg matrix in situ composites fabricated by spark plasma sintering. *Metals* **2017**, *7*, 358. [CrossRef]
178. Lin, D.-J.; Hung, F.-Y.; Lee, H.-P.; Yeh, M.-L. Development of a novel degradation-controlled magnesium-based regeneration membrane for future guided bone regeneration (GBR) therapy. *Metals* **2017**, *7*, 481. [CrossRef]
179. Vinogradov, A.; Vasilev, E.; Kopylov, V.I.; Linderov, M.; Brilevesky, A.; Merson, D. High performance fine-grained biodegradable Mg-Zn-Ca alloys processed by severe plastic deformation. *Metals* **2019**, *9*, 186. [CrossRef]
180. Tun, K.S.; Zhang, Y.; Parande, G.; Manakari, V.; Gupta, M. Enhancing the hardness and compressive response of magnesium using complex composition alloy reinforcement. *Metals* **2018**, *8*, 276. [CrossRef]
181. Bakhsheshi-Rad, H.R.; Dayaghi, E.; Ismail, A.F.; Madzlan, A.Z.I.Z.; Akhavan-Farid, A.; Xiongbiao, C. Synthesis and in-vitro characterization of biodegradable porous magnesium-based scaffolds containing silver for bone tissue engineering. *Trans. Nonferrous Met. Soc. China* **2019**, *29*, 984–996. [CrossRef]
182. Razzaghi, M.; Asgarani, M.K.; Bakhsheshi-Rad, H.R.; Ghayour, H. In vitro degradation, antibacterial activity and cytotoxicity of Mg-3Zn-xAg nanocomposites synthesized by mechanical alloying for implant applications. *J. Mater. Eng. Perform.* **2019**, *28*, 1441–1455. [CrossRef]
183. Bakhsheshi-Rad, H.R.; Hamzah, E.; Staiger, M.P.; Dias, G.J.; Hadisi, Z.; Saheban, M.; Kashefian, M. Drug release, cytocompatibility, bioactivity, and antibacterial activity of doxycycline loaded Mg-Ca-TiO2 composite scaffold. *Mater. Des.* **2018**, *139*, 212–221. [CrossRef]
184. Bakhsheshi-Rad, H.R.; Abdellahi, M.; Hamzah, E.; Daroonparvar, M.; Rafiei, M. Introducing a composite coating containing CNTs with good corrosion properties: Characterization and simulation. *RSC Adv.* **2016**, *6*, 108498–108512. [CrossRef]
185. Bakhsheshi-Rad, H.R.; Hamzah, E.; Tok, H.Y.; Kasiri-Asgarani, M.; Jabbarzare, S.; Medraj, M. Microstructure, In Vitro corrosion behavior and cytotoxicity of biodegradable Mg-Ca-Zn and Mg-Ca-Zn-Bi alloys. *J. Mater. Eng. Perform.* **2017**, *26*, 653–666. [CrossRef]
186. Bakhsheshi-Rad, H.R.; Hamzah, E.; Farahany, S.; Staiger, M.P. The mechanical properties and corrosion behavior of quaternary Mg-6Zn-0.8Mn-xCa alloys. *J. Mater. Eng. Perform.* **2015**, *24*, 598–608. [CrossRef]
187. Tok, H.Y.; Hamzah, E.; Bakhsheshi-Rad, H.R. The role of bismuth on the microstructure and corrosion behavior of ternary Mg-1.2Ca-xBi alloys for biomedical application. *J. Alloys Compd.* **2015**, *640*, 335–346. [CrossRef]
188. Bakhsheshi-Rad, H.R.; Hamzah, E.; Fereidouni-Lotfabadi, A.; Daroonparvar, M.; Yajid, M.A.M.; Mezbahul-Islam, M.; Kasiri-Asgarani, M.; Medraj, M. Microstructure and bio-corrosion behavior of Mg–Zn and Mg–Zn–Ca alloys for biomedical applications. *Mater Corros.* **2014**, *65*, 1178–1187. [CrossRef]
189. Bakhsheshi-Rad, H.R.; Idris, M.H.; Abdul-Kadir, M.R.; Ourdjini, A.; Medraj, M.; Daroonparvar, M.; Hamzah, E. Mechanical and bio-corrosion properties of quaternary Mg–Ca–Mn–Zn alloys compared with binary Mg–Ca alloys. *Mater. Des.* **2014**, *53*, 283–292. [CrossRef]

190. Bakhsheshi-Rad, H.R.; Abdul-Kadir, M.R.; Idris, M.H.; Farahany, S. Relationship between the corrosion behavior and the thermal characteristics and microstructure of Mg–0.5Ca–xZn alloys. *Corros. Sci.* **2012**, *64*, 184–197. [CrossRef]
191. Bakhsheshi-Rad, H.R.; Idris, M.H.; Abdul Kadir, M.R.; Farahany, S. Microstructure analysis and corrosion behavior of biodegradable Mg–Ca implant alloys. *Mater. Des.* **2012**, *33*, 88–97.
192. Farahany, S.; Bakhsheshi-Rad, H.R.; Idris, M.H.; Kadir, M.R.A.; Lotfabadi, A.F.; Ourdjini, A. In-situ thermal analysis and macroscopical characterization of Mg–xCa and Mg–0.5Ca–xZn alloy systems. *Thermochim. Acta* **2012**, *527*, 180–189. [CrossRef]
193. Daroonparvar, M.; Yajid, M.A.M.; Yusof, N.M.; Bakhsheshi-Rad, H.R. Preparation and corrosion resistance of a nanocomposite plasma electrolytic oxidation coating on Mg-1%Ca alloy formed in aluminate electrolyte containing titania nano-additives. *J. Alloys Compd.* **2016**, *688*, 841–857. [CrossRef]
194. Safari, N.; Toroghinejad, M.R.; Kharaziha, M. Influence of copper on the structural, mechanical, and biological characteristics of Mg–1Al–Cu alloy. *Mater. Chem. Phys.* **2019**, *237*, 121838. [CrossRef]
195. Golshirazi, A.; Kharaziha, M.; Golozar, M.A. Polyethylenimine/kappa carrageenan: Micro-arc oxidation coating for passivation of magnesium alloy. *Carbohydr. Polym.* **2017**, *167*, 185–195. [CrossRef]
196. Wierzbicka, E.; Pillado, B.; Mohedano, M.; Arrabal, R.; Matykina, E. Calcium doped flash-PEO coatings for corrosion protection of Mg alloy. *Metals* **2020**, *10*, 916. [CrossRef]
197. Feliu, S., Jr. Electrochemical impedance spectroscopy for the measurement of the corrosion rate of magnesium alloys: Brief review and challenges. *Metals* **2020**, *10*, 775. [CrossRef]
198. Mitchell, J.; Crow, N.; Nieto, A. Effect of surface roughness on pitting corrosion of AZ31 Mg alloy. *Metals* **2020**, *10*, 651. [CrossRef]
199. Liu, H.; Li, W.; Pei, Z.; Yan, M. Mg-based materials with quasiamorphous phase produced by vertical twin-roll casting process. *Metals* **2020**, *10*, 452. [CrossRef]
200. Qi, Y.; Wang, H.; Chen, L.; Zhang, H.; Chen, G.; Chen, L.; Du, Z. Preparation and mechanical properties of ZK61-Y magnesium alloy wheel hub via liquid forging—Isothermal forging process. *Metals* **2020**, *10*, 385. [CrossRef]
201. Kunčická, L.; Král, P.; Dvořák, J.; Kocich, R. Texture evolution in biocompatible Mg-Y-Re alloy after friction stir processing. *Metals* **2019**, *9*, 1181. [CrossRef]
202. Chen, Y.-T.; Hung, F.-Y.; Syu, J.-C. Biodegradable implantation material: Mechanical properties and surface corrosion mechanism of Mg-1Ca-0.5Zr alloy. *Metals* **2019**, *9*, 857. [CrossRef]